POLITECNICO DI TORINO

Department of Applied Science and Technology

Master's degree

in Mechanical Engineering

Master Thesis

Analysis of Historical Steel Artefacts

Supervisors

Signature of the supervisors

prof. Matteis Paolo

prof. Scavino Giorgio

Candidate

Signature of the Candidate

Alessandro Eren Boccardo

Abstract

The goal of this work is to study the microstructure and the production process of historical steels.

Two tie-rods fragments, probably fabricated in the XVII century, and a XVI century sword, were examined, mainly by means of optical metallography and microhardness testing. Moreover, a second phase extraction and analysis procedure have been attempted, and a thermo-metallurgical model of a possible partial quenching and self-tempering heat treatment of the sword have been developed.

Index

1 Introduction

The goal of this work is to investigate the production methods of steel artefacts produced in a timeframe between the end of the Medieval era (1500) and before the 1st industrial revolution (1760).

This will be accomplished by studying on one hand the making of high-quality materials such as an XVI century sword and other hand more simpler materials like the case of a masonry tie-rod.

The tie-rod comes from the civil engineer world and it has been produced just before the 1760.

The necessary permissions to study the XVI century sword have been granted to Polito from the Museum of Arms of Brescia thanks to the sword's bad corrosion state. Nonetheless, it is a great example of northern Italy late Medieval swordsmanship amazing abilities.

Since in the period of investigation the art of steelmaking and blacksmithing was surrounded by secrets shared most often only from father to son not many historical metallographic descriptions of the production processes came to our times.

Consequently, both specimens will be analysed both with destructive and non-destructive methods.

For this scope, an optical microscope will be used before to study the inclusion distribution and after etching to inspect the metallographic microstructure.

Knowledge of the microstructure impurities present in the steel could lead to interesting insight about the initial iron ore composition.

In fact, even if the steelmaking process will for sure affect the composition of the impurities it is also true that there are some elements that get altered in a similar way and we can hypnotize that their relative percentage will stay close to the one in the starting ore.

For this reason, a second phase extraction experiment followed by an EDS analysis at the SEM microscope will be object of study.

Moreover, to get some more information regarding the hardness of the specimens, their micro-hardness will get tested. This test will also act as a double-check to characterize the metallographic microstructures in a more definite way.

The thesis will start with an introduction to the Ancient metallurgy processes.

This chapter will be dedicated to topic such as the different steelmaking techniques known to the period in inquisition, the iron ore, the slag, and the various heat treatments of steel.

Afterwards it will be easier to understand the various reconstructions of the production process of the artefacts subject of this work.

On this topic, a FEM Thermal-Phase model of the quenching and self-tempering of the sword will be created thanks to the commercial software COMSOL and Solidworks to go deeper in details of the XVI sword manufacturing process.

Acknowledgements

I would like to thank my supervisors Professor Matteis Paolo, Prof. Scavino Giorgio and Marco Merlo for their guide, patience, and feedbacks through this work and for the opportunity.

And, I should thank the Museo delle Armi di Brescia because without their permission I couldn't study the G59 sword.Another thanks goes to my parents Giuseppe and Serap for their sacrifices and to my girlfriend Vanessa for her support.

2 Ancient Metallurgy Processes

2.1 Introduction

This chapter briefly describes the main production and processing techniques of the steel made between the end of the Medieval era (1500) and before the 1st industrial revolution (1760) to better understand the observations made on the tie-rod bar as well as on the XVI century sword that will be discussed in the next chapters.

Specifically, we will touch on each step of the production process from the mineral to the final good. In fact, steel is present on Earth in the form of minerals(ore).

Additionally, it will be discussed the role of metallic inclusions regarding the manufacturing process and the quality of the steel.

Moreover, the forging and quenching process will be briefly described as they are of particular interest for the production of the artefacts presented in this work.

Many studies have been devoted to the research of the production process of historical artefacts in fact the last chapter of this section will cite some of previous research particularly relevant for this thesis.

2.2 The Iron ore

In the world iron is most present in form of iron ores such as magnetite (Fe_3O_4, 72.4% Fe), hematite (Fe_2O_3, 69.9% Fe), goethite (FeO (OH), 62.9% Fe), limonite (FeO (OH)·n(H2O),55% Fe) or siderite (FeCO3, 48.2% Fe). (1)

Usually, these iron oxides are found mixed with other worthless non-metallic material called gangue.

In the direct method of steel making for example portions of this gangue gets inevitably introduced to the furnace where it will form the inclusions.

For this reason, the iron ore, before being inserted in the furnace, gets shattered in really fine grains and washed to reduce the gangue presence to the minimum. This procedure is known as mineral processing, mineral dressing, or ore dressing.

Another metallurgical process to purify the metal from possible unwanted elements is called **roasting**. This process requires at high temperature(200-300°C) in presence of air(oxygen) and it consist in a thermal gas-solid reaction. It is generally applied to minerals that presents sulphur type impurities.

After the reaction takes place gas sulfuric dioxide gets generated and can be easily expelled from the furnace to obtain a purer metal.

$$2MS(s) + 3O_{2(g)} \rightarrow 2MO(s) + 2SO_{2(g)}$$

The study of an ancient steel's non-metallic impurities can sometimes track back the extraction mines from which it came from since these impurities are usually connected with the presence of a particular element in a specific extracting mine. (2)

Most of the methods in the scientific literature (3) (4) require a large-scale statistical analysis that require a vast number of samples. Unfortunately, the number of specimens that can be studied is not always enough to be statistically relevant especially considering the rarity of some historical artefacts.

The main ore mining extraction point of the late medieval and before the 1st industrial revolution are known from historical documentations of the time.

In Italy in particular the main Lombard iron rich deposit largely utilized in the late medieval era can be seen in the Figure 2.2-1.

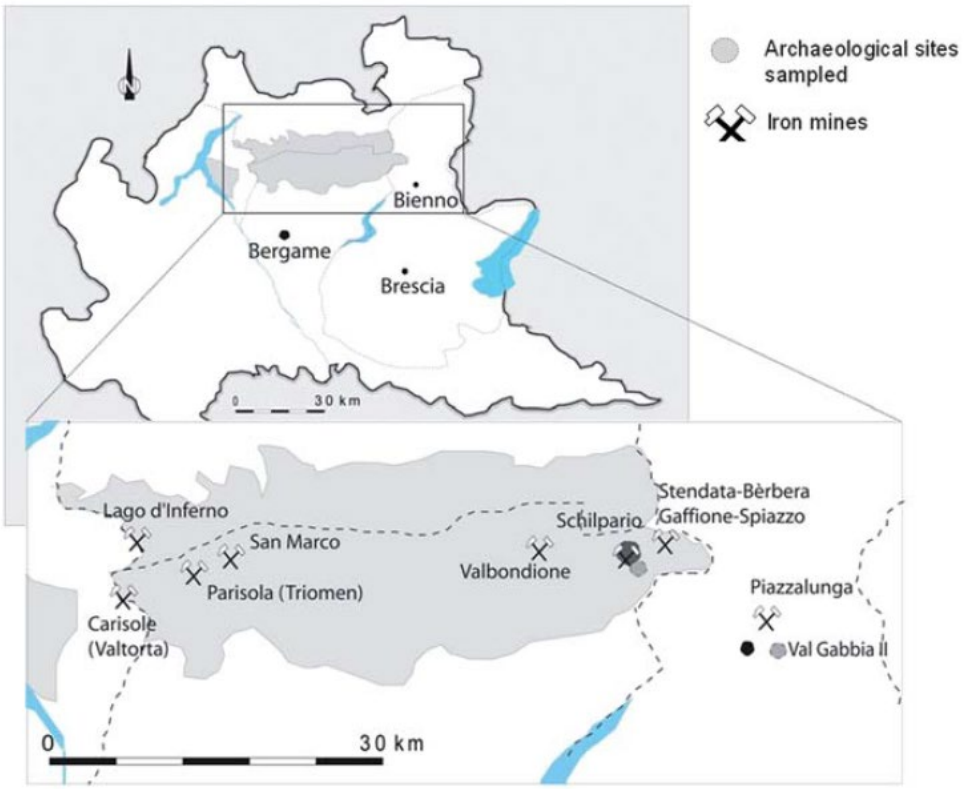

Figure 2.2-1 Location of the iron mines and archaeological sites sampled in Lombardy. (5)

2.3 Direct Method

The direct method or bloomery is the oldest steel production methods in the history of mankind. (6)

It consists in inserting iron ore and charcoal inside a furnace. The temperature would then be increased and kept approximately constant by means of a blower in order to start the solid-state reduction act to obtain the bloom. (Figure 2.3-2)

Figure 2.3-1 Blacksmith producing steel from the furnace (7)

The higher the temperature the higher the better the carbon diffusion phenomena and the hither carbon percentage in the resulting bloom. The bloom is a sort of very porose iron sponge.

It is possible that the bloom contains also other elements that reduced inside the furnace. For example, S and P if present can reduce the mechanical proprieties of the material so they must be avoided.

Moreover, the carbon percentage of the obtained iron can be further increased reinserting the bloom into the furnace. In fact, the high temperatures of the furnace and the presence of a carbon atmosphere derived by the charcoal will allow carbon diffusion inside the material thus increasing carbon percentage.

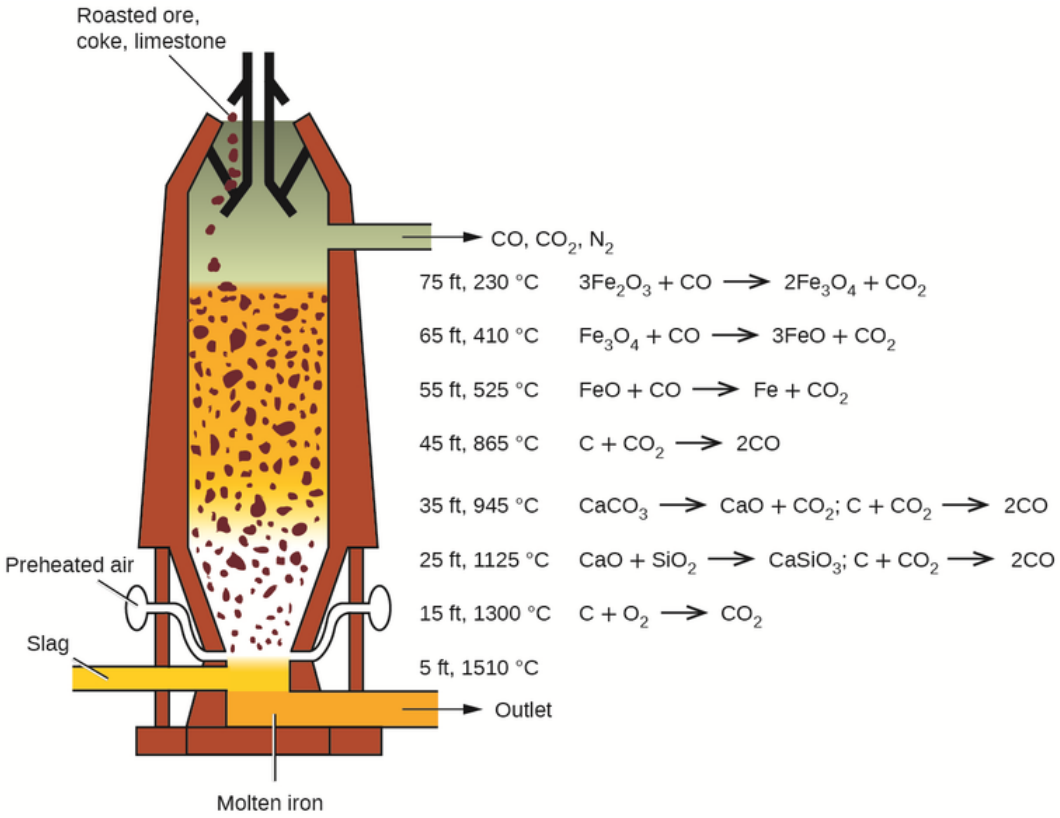

Figure 2.3-2 Furnace for iron smelting and Chemical Reaction taking place at different temperature. (8)

Unfortunately, the carbon diffusion obtained with this method follows a linear gradient. Specifically, the parts of the material directly in contact with the carburizing atmosphere will have higher carbon percentages then the ones further away.

This process was the most popular method at the end of the Medieval era.

2.4 Indirect Method

In Italy during the XV-XVI centuries there were many blast furnaces especially around Brescia. On the other hand in Europe the first iron production furnaces can be dated back to

the XIV century. During the first industrial revolution the main innovation to this method was to use coke instead of charcoal.

This method gained more and more popularity later in the 1856 with the invention of the Bessemer converter became the main method for steel production. (11)

The indirect method of steel production involved 2 steps: (9)

1) Adding Carbon
2) Removing Carbon

The process starts by inserting the iron ore inside a large furnace at a very high temperature. Inside the furnace there is a large quantity of charcoal that creates a carbon rich atmosphere. This carbon atmosphere diffuses in the ore specifically inside the iron core increasing its relative carbon percentage. As the carbon percentage increases locally the melting temperature also decreases making the iron core literally bleed cast iron.

The result of this process is the so called 'pig iron' (10) .This has a really high carbon percentage and unfortunately also impurities such as P and S produced during the making. For those reasons, the bloom gets inserted again in another furnace where it is subject to an oxygen flow from a blower in order to transform the carbon in carbon dioxide and decreasing the overall carbon percentage of the bloom.

This step is then repeated until the desired carbon percentage is reached.

Overall, this process takes around 5 hours and a portion of iron get lost in oxidation in the second step amounting to a loss of 23-24% of carbon loss.

2.5 Slag inclusion composition

The end product of both the metal production processes discussed in the previous chapters is the so-called wrought iron (low-carbon iron) and lots of impurities(slag) are present.

The term “slag” describes in steelmaking is usually a mixture of metal oxides and silicon dioxide. (12)

Most commonly the slag can be found in the form of basic oxides (CaO, MgO, MnO) or acidic oxide(SiO_2, P_2O_5).

Wrought iron usually contains extremely inhomogeneous carbon content as well as in slag inclusion distribution. (13)

In fact, the slag produced by *Direct and Indirect methods* can be distinguished.

For example, the direct method produces large quantities of oxides that could not be reduced in the furnace like the ones present in Table 1.

Table 1 Direct method/Blooomery slag most common oxides. (3)

	MgO	Al_2O_3	SiO_2	K_2O	CaO	TiO_2	SrO	BaO
Bloomery slag	●	●	●	●	●	●	●	●
Clay		●	●	●		●		●
Fuel ash	●			●	●		●	
Smithing flux			●					

On the other hand, the *Indirect Method* should produce greater quantities of oxides created during the re-oxidation process such as of phosphor oxides for example. (13)

Insight of this an EDS (see chapter 2) analysis could help identify the production process and sometimes even the mining zone of the ore. (3)

However, the different production parameters or the addition of alloying elements (intentional or unintentional) could lead to very diverse compositions in the final slag inclusions.

Hence this method does not give absolute certainties but only hints that can be correlated with a multidisciplinary approach to get a bigger picture regarding a particular steel’s history.

2.6 Forging

Forging consists in hammering a hot metal in order to plastically deform and remove impurities like inclusions. (Figure 2.6-1)
This process gives the shape to the sword provoking orientation in the grain, inclusions and overall metallographic structures presents in the material.

Figure 2.6-1 Swordsmith forging a blade (14)

2.7 Carburization

The carburization is a process used to diffuse (Figure 2.7-1) carbon into the steel with the scope of having a hard external surface and a thought internal volume of the material. The material is inserted in a furnace with a carbon atmosphere and increasing the temperature the diffusion starts,

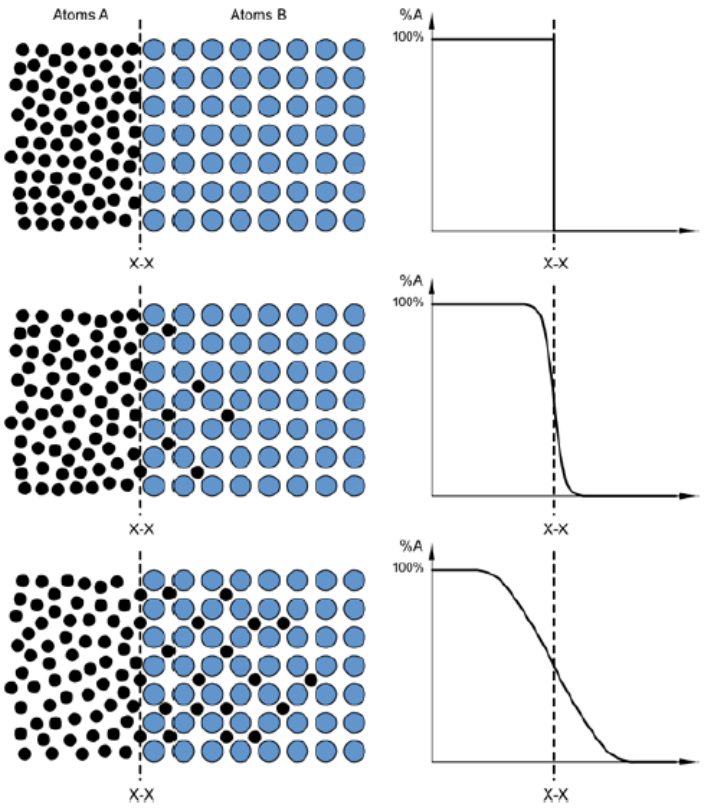

Figure 2.7-1 Inter-diffusion for lattice interstitial sites in a heterogeneous system between a gas and a solid. (15)

2.8 Heat Treatments

Quenching is a process of quickly cooling a metal after reaching complete the austenitization temperature A_3.This temperature depends on the percentage of carbon present in the material (Figure 2.8-1).

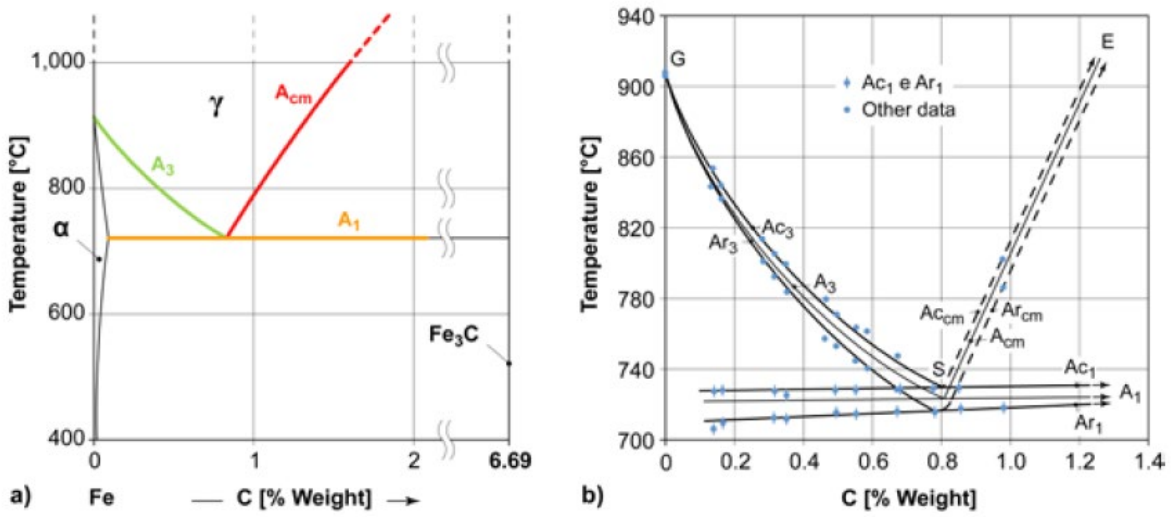

Figure 2.8-1 Critical points of the Fe-C phase diagram. Note that A3 depends on %C in weight. (16)

The selection of the quenchant medium it is connected to the hardenability of the material, the section dimensions and the cooling rated required to obtain the desired microstructure.

In the end of the Medieval era the quenchant medium was typically water for fast cooling rates while oil for slower cooling rates.

The **blacksmiths** of that era had many different recipes for the quenchant medium.

An example of quenching of a steel rod is presented in Figure 2.8-3.

The result of quenching is Martensite, a really hard but brittle metallographic structure similar to ferrite but taller.

In order to decrease the brittleness of **Martensite** and increase toughness the material usually undergoes a tempering heat treatment right after the quenching.

Tempering consists in increasing the temperature of the material before A1 in order to transform Martensite in tempered martensite. (Figure 2.8-2)

The former has a lower hardness than Martensite but it is more thought.

The effects of tempering at different tempering temperature are reported in the Figure 2.8-2 [5]

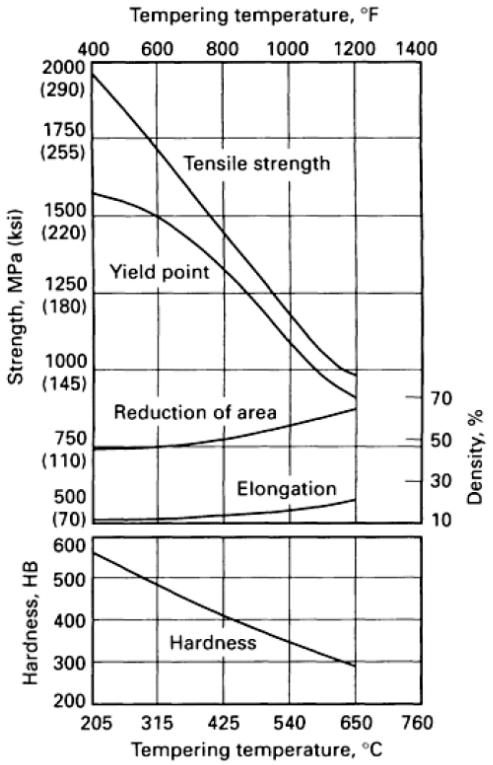

Delayed Quenching is the practice of cooling the material first in air for a small timeframe before quenching it.

This leads to transform part of the austenite in ferrite and then the remaining austenite to martensite.

Of course, the centre cools down more slowly so will be the centre of the ferrite transformation leading to obtain a though heart(ferrite) surrounded by a hard surface(martensite).

Partial Quenching is the process of extracting the material from the quenchant medium before complete cooling. Again, the centre remains at a higher temperature then the outside surface leading to a sort of tempering that decrease the brittleness and increase the toughness of the martensite. With this particular quenching method, we could obtain Bainite in the centre zones if the temperature is high enough for a long enough period that could be decided looking at an experimental TTT diagram for example.

Complete Quenching and tempering are the practice of quenching and then tempering at different temperature levels chosen by the blacksmith.

In the case of swords, a popular tempering technique is the so called self-tempering where the sword is immersed in the quenchant medium of for 4/5 of its length and extracted before complete cooling of the material.

Now since the tang is way warmer than the tip of the blade it will temper the blade with a linear gradient. This leads to obtain a more thought tang and bas of the sword and a harder tip ready to engage in a battle.

In old steels the small presence of alloying elements within the material makes it really difficult to quench because the lower the alloying elements the higher the cooling rate must be so a mistake a some seconds could lead to a complete failure of the process.

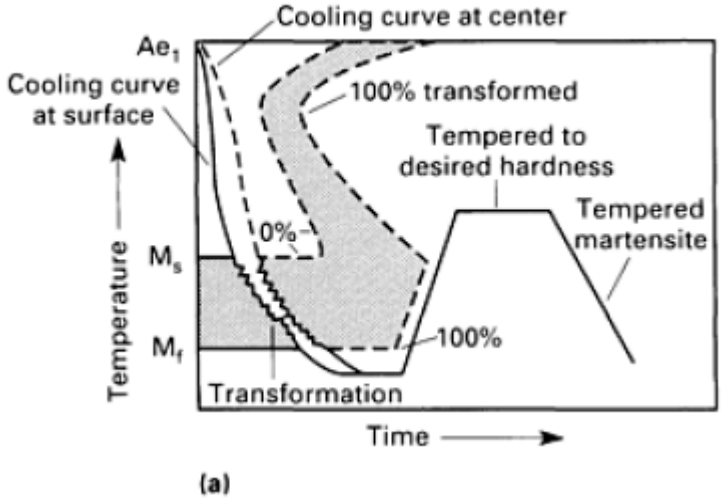

Figure 2.8-2 Conventional quenching and tempering processes that use oil or water quenchants. (17)

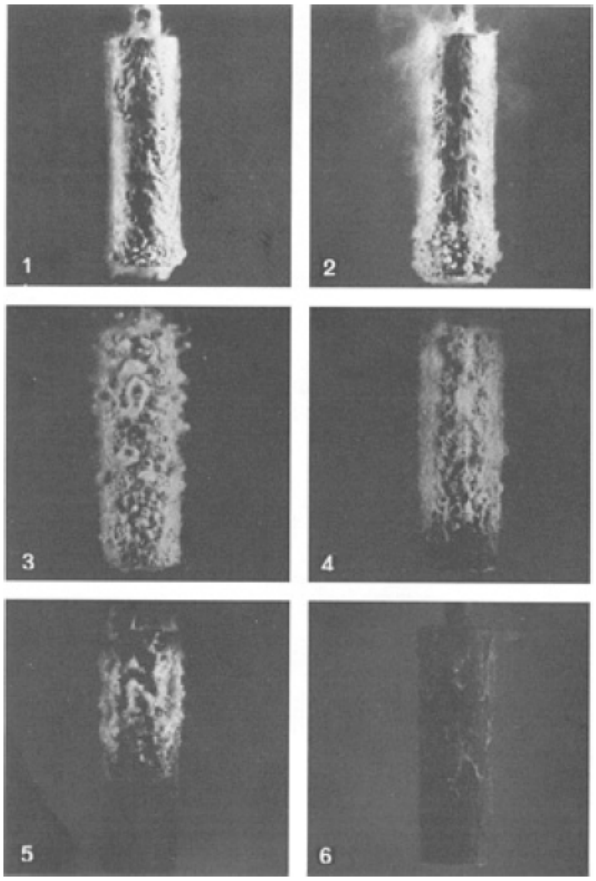

Figure 2.8-3 Photo sequence of a hot steel rod being quenched (17)

2.9 Previous work on the Subject

Archaeometallurgy is vast research field that aims to reconstruct the history of steel made objects such as arms, swords and even tie-rods for example.

Everything that is written in this thesis comes either from scientifical evidence or from a number of studies known in the literature.

When analysing the tie- rods for example the work of Prof Matteis and Prof. Scavino on "Characterization and Joining of an Historical Ferrous Tie-Rod" and "Mechanical Performance of historical wrought iron rods" have been really helpful.

Also, the book of ‘Armi Bianche dal Medioevo all’Età Moderna’ of Carlo de Vita helped to understand the style of the XVI sword.

Another important influence came from the thesis of Roberto Pallaro that did a really in-depth analysis of a sword similar to mine.

There are also many other sources that will be attached to the biography.

3 Analysis of Historical Wrought Iron Rods

3.1 Introduction: The Tie-Iron in Examination

The goal of this metallographic analysis is to analyse the microstructure of a civil engineer steel dated just before the 1st industrial revolution.

In particular the iron-rod belongs to historical masonry buildings in the city of Turin, Italy. This time period was characterized by the use of both direct and indirect processes for steelmaking.

During the metallographic analysis, the specimens will be first inspected before etching in order to see clearly the inclusion distribution. After the nital etching the microstructures will be identified at the optical microscope.

Later to double check on the identified microstructures in the previous step the specimen will get localized hardness analysis.

Finally, in order to find out which method was used the following chapters will propose a metallographic analysis, a micro hardness analysis and a EDS analysis.

Figure 3.1-1 Masonry building in Turin where the iron tie-rod came from. (13)

3.2 Sampling

The iron rod has a cylindrical shape and two pieces have been cut on the top(01-PI-TO) and the bottom(04-PI-TO).

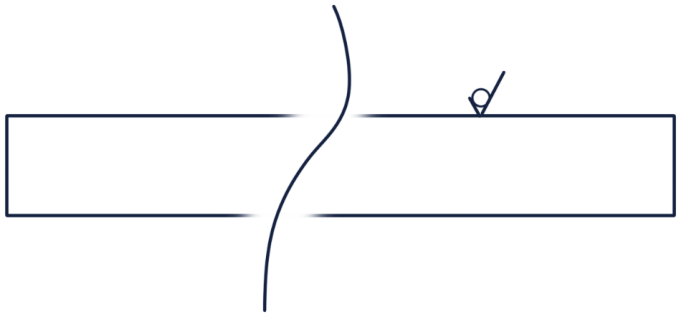

Figure 3.2-1 Specimen look and cut.

3.2.1 The Cutting Operation

A **quick disk cutting tool** has been used to cut a slice to obtain a slice of the material and start the grinding process. (**Figure 3.2-2** Quick disk cutting)

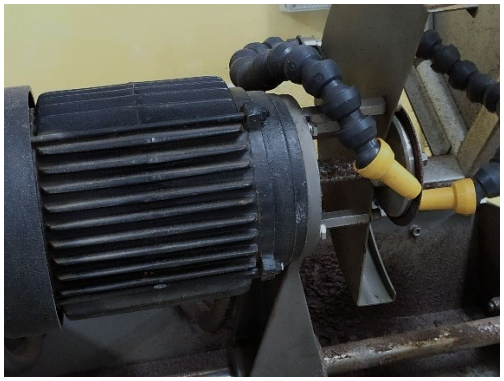

Figure 3.2-2 **Quick disk cutting tool.**

3.2.2 Grinding Process

Since the sample might have lots of *undulations* or *curvatures* coarse, **abrasive papers** (from 60 to 4000) combined **with diamond paste abrasives** (Figure 3.2-3) together with proper lubrification systems have been employed to generate a flat surface over the sample.

Figure 3.2-3 Diamond abrasive pastes on the left and centre. Abrasive paper on the right.

Low roughness will also benefit the measurement of hardness that will be discussed in the following chapters.

The abrasion process has been carried on a **workstation (Figure 3.2-5)** equipped with **water and refrigerant** supply plus a **moving disk** where the abrasive papers get dressed upon.

In this step is important to apply small forces and have all the scratch lines on the specimen with the same common direction.

The importance of using the right polishing tehnique for the right amount of time can be described by the the picture below.(Figure 3.2-4)

Fig. 18 **Fig. 19**

Pearlitic steel. Fig. 17: results of abrading on an abrasive belt and then polishing for only long enough to remove abrasion scratches; structure contains abrasion-deformation artifacts. Fig. 18: results of abrading on 600-grit silicon carbide paper and then polishing only long enough to remove abrasion scratches; kinking of cementite plates is an abrasion-deformation artifact. Fig. 19: results of abrading on 600-grit silicon carbide paper and polishing for a longer time than for Fig. 18. Figure 19 shows the true structure. Picral. 2000×

Figure 3.2-4 Figure taken from (18)

Thus, *gradually increasing the fineness* of the rotating abrasive down to **1μm** the specimen was all set for the nital attack. (**Figure 3.2-6**)

Figure 3.2-5 Workstation, specimen, water, and refrigerant lubricant.

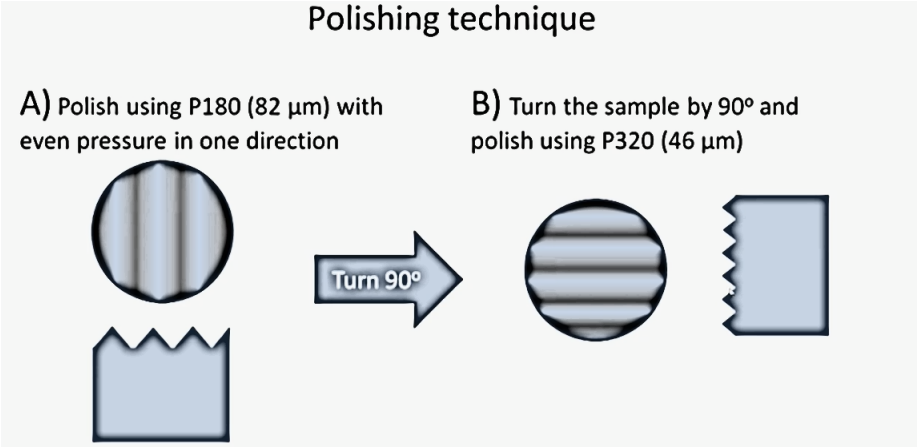

Figure 3.2-6 Polishing Technique. (19)

3.2.3 Nital Etching

"**Nital** is a solution *of nitric acid and alcohol* commonly used for etching of metals. It is especially suitable for revealing the *microstructure of carbon steels*. The alcohol can be methanol, ethanol or methylated spirits." (20)

The alcohol of choice for this experiment was **ethanol**.

The specimen has been washed with a solution of **Nital @3% in volume** for 30 seconds and after with ethanol.

3.3 Metallographic Macrostructural and Microstructural Analysis

3.3.1 Introduction

This subchapter introduces briefly the technology used for metallographic microstructure identification.

In an **inverted incident-light microscope** like the one used for our study the specimen is placed with its polished plane inverted during observation. This allows the light to hit it and bounce.

back to a screen or through a series of prisms and **mirrors** to the eye of the observer.

Since the *depth of field* of the **optical microscope** (Figure 3.3-1) is a few µm thus it is clear

that having a flat sample is of vital importance to see clear images. (Figure 3.3-4)

Reflection of light is used to study metals.

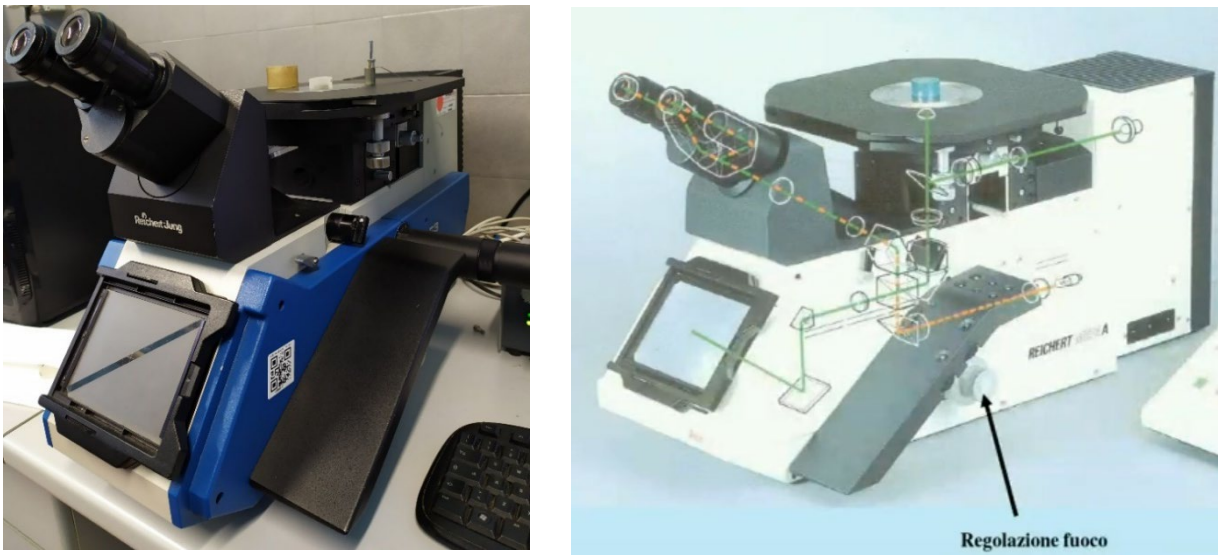

Figure 3.3-1 On the left: Optical microscope used for the metallographic inspection, On the right: Microscope working principle (21)

The **objective lens** is one of the most important components of the optical microscope since it

combines the light from the specimen to produce the final image.

Notably during the metallographic study, it is needed to change the lens to **zoom** in and out

from the material to investigate particular microstructures. (Figure 3.3-2)

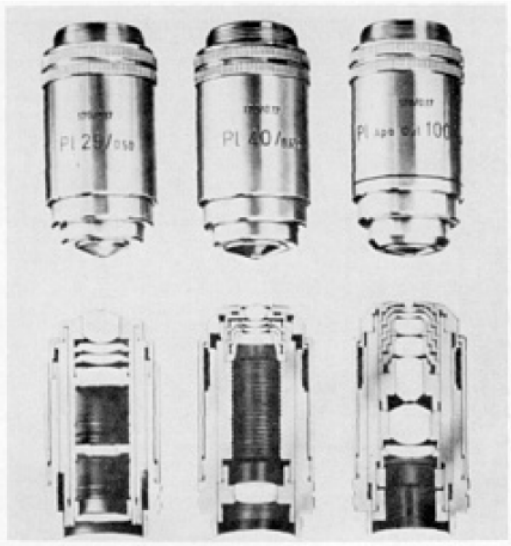

Figure 3.3-2 Series of lenses for microscopes at different focal lengths. (18)

Other than changing the lens, the focus and the position of the sampled image it is also possible to change the amount of light hitting the surface of the sample in order to increase contrast and lower the exposure to reveal details before hidden. (Figure 3.3-3)

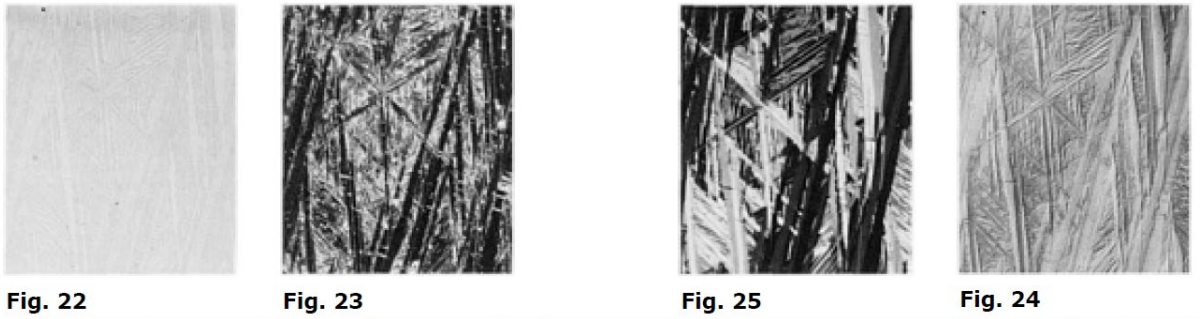

Cu-11.8Al (aluminum bronze), heat treated, with martensite in the microstructure. Fig. 22: bright-field illumination. Fig. 23: dark-field illumination. Fig. 24: differential interference-contrast illumination. Fig. 25: crossed polarized light illumination. As-polished. 200×

Figure 3.3-3 Example on the influence of light level on the final image. (18)

Before been able to check the microstructure of our material at the microscope a **nital** etching is needed to expose the grain boundaries for possible Pearlite because it presents very thin lamellae that the microscope may have difficulties resolve. (Figure 3.3-4)

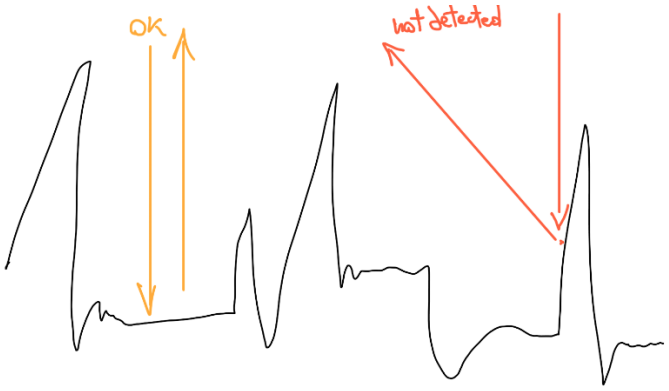

Figure 3.3-4 Light detection in function of the rugosity of the material. A flat surface=low rugosity (yellow light beam) reflects better thus giving a better picture than a surface with high rugosity where the signal gets simply lost. (red light beam)

Moreover, a series of **grinding operations** will be performed to guarantee a **flat** specimen. In fact, decreasing the rugosity increases the chances of light waves to be reflected perfectly and being captured by our microscope sensor for an accurate reading.

3.3.2 01-PI-TO

The macrostructure of the sample **01-PI-TO** is divided in 2 zones that can be seen in Error! Reference source not found. .

The two different zones of *01-PI-TO* (Figure 3.3-6) show a very non-homogeneous structure both in terms of carbon percentage and inclusion distribution.

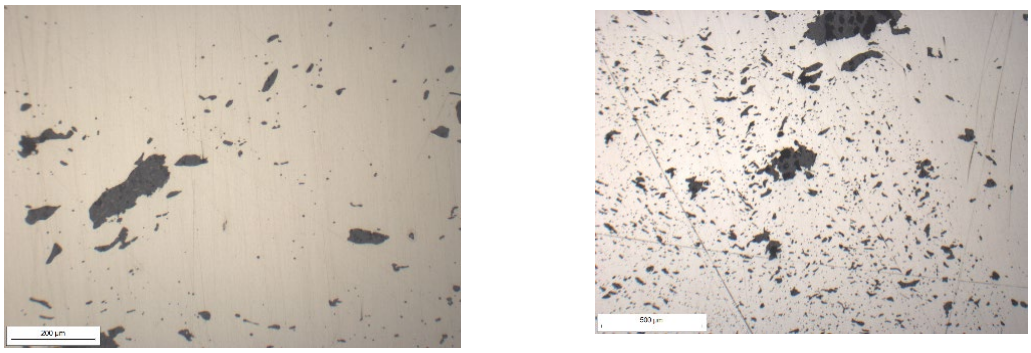

Figure 3.3-5 Inclusion distribution in A (left) and B(right) shows the different inclusion distribution.

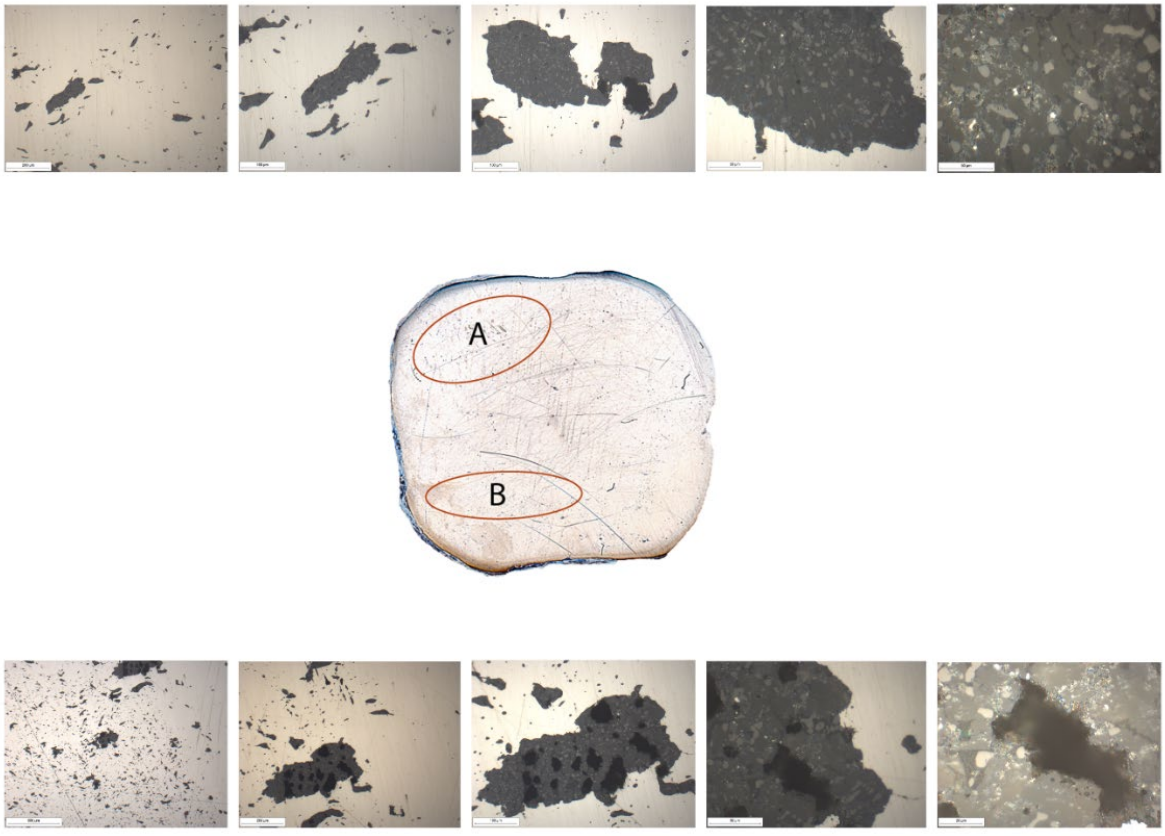

Figure 3.3-6 01-Pi-TO Microscopy Photos at different scale of the zone A(Top) and zone B (Bottom)

On the other hand, the two different areas (Figure 3.3-7) after nital attack show the following microstructures:

- **A**: Ferrite + inclusions
- **B**: Ferrite + Perlite

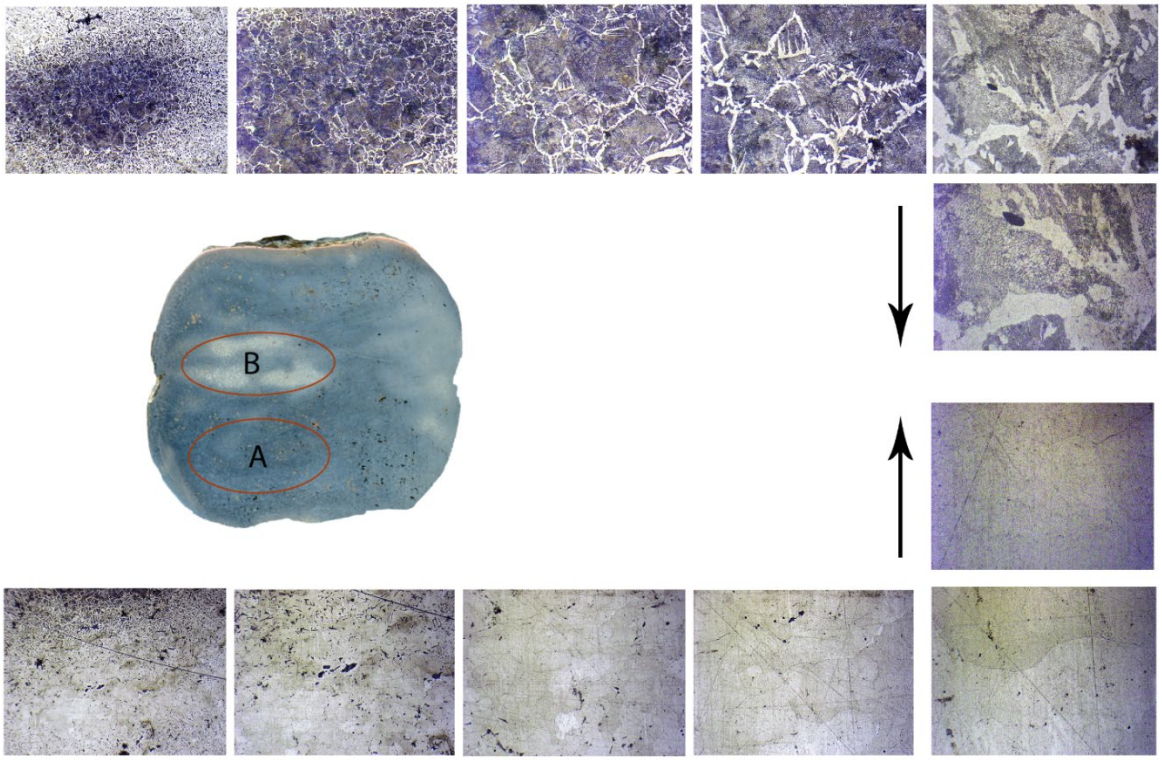

Figure 3.3-7 01-PI-TO Microscopy Photos at different scale of the zone B(Top) and zone A (Bottom) after nital attack

Looking at **Zone A** from Figure 3.3-8 it shows a white reflecting surface that is traceable to **ferrite** while a couple of black dots that should be small **inclusions** or *even perlite*.

Moreover those microstructure suggest slow cooling.

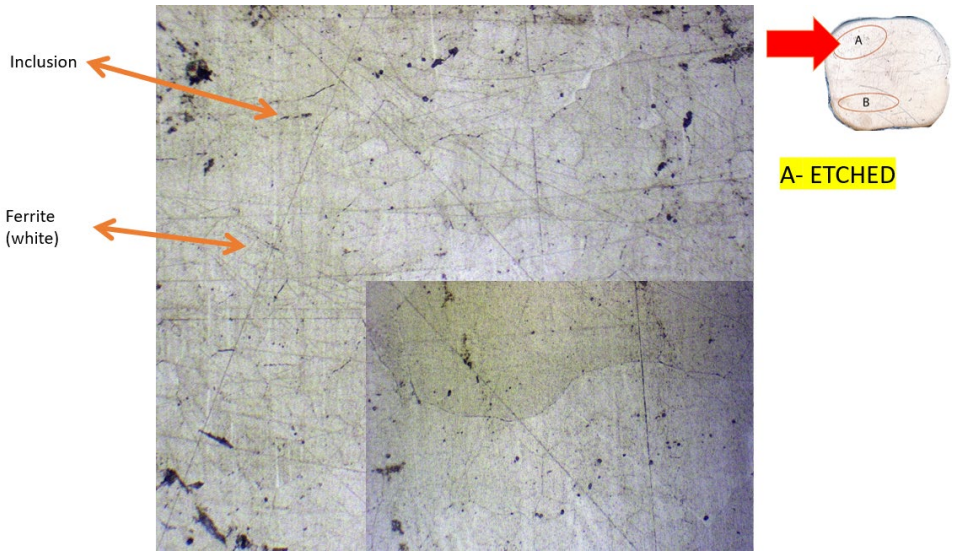

Figure 3.3-8 Zone A 01-PI-TO shows ferrite(white) and cementite(black)

On the other hand, as it can be seen in the image below **zone B** have the clear lamellae structures of **Pearlite** and the grain boundaries are made of **Ferrite**.

The formation of pearlite can be ascribed to a slow cooling in the production process.

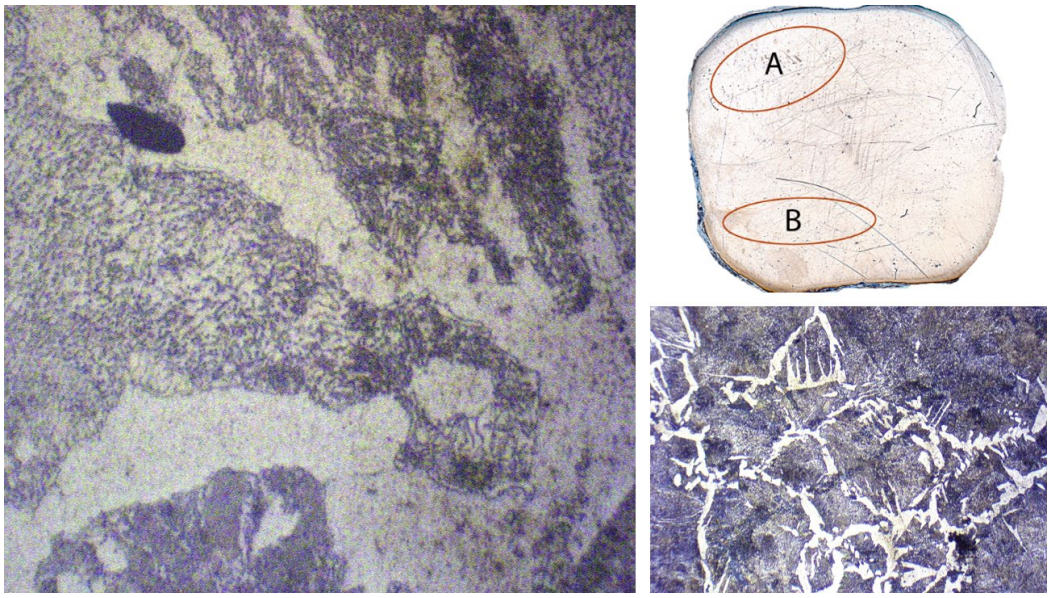

Figure 3.3-9 Zone B 01-PI-TO Pearlitic lamellae colonies surrounded by hypereutectic cementite at the grain boundaries. There is also some Widmannstetter ferrite α_w.

However, to be 100% sure about the phases present in the material it is mandatory to etch it with nital.

Notably to expose pearlite because it can happen that the lamellae are so close to each other that the microscope resolution cannot even detect them. (Figure 3.3-10).

In fact, the acid reacts with the ferrite present in the lamellae while the cementite (high carbon zone) present in the pearlite does not react causing then indentations between the various lamellae and increase detectability of the latter with the optical microscope. (Figure 3.3-9)

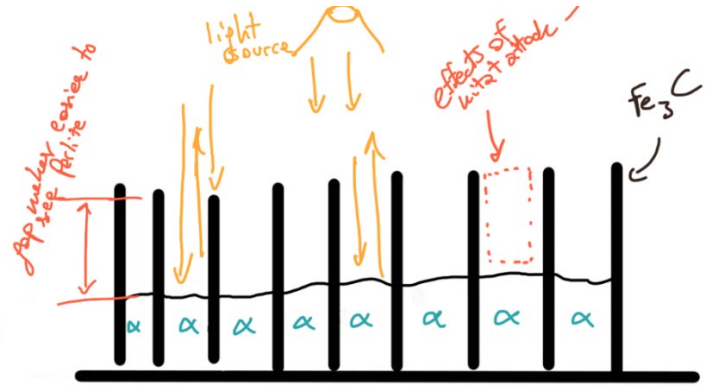

Figure 3.3-10 Effects of nital attack on Pearlite surface

Overall considering a macro-scale the great difference in carbon percentage of the different zones could be caused by temperature gradients during the final forging process.

In fact, during such process the operator forges on one side hand of the cylinder(hot) while the other side of the bar gets colder.

3.3.3 04-PI-TO

The macrostructure of the sample **04-PI-TO** is divided in 2 zones that can be seen in **Figure 3.3-11.**

The two different zones of *04-PI-TO* showed again a very non-homogeneous structure both in terms of carbon percentage and inclusion distribution.

Overall Zone B of 04-PI-TO show a much lower inclusion presence as well as carbon percentage compared to Zone B of 01-PI-TO.

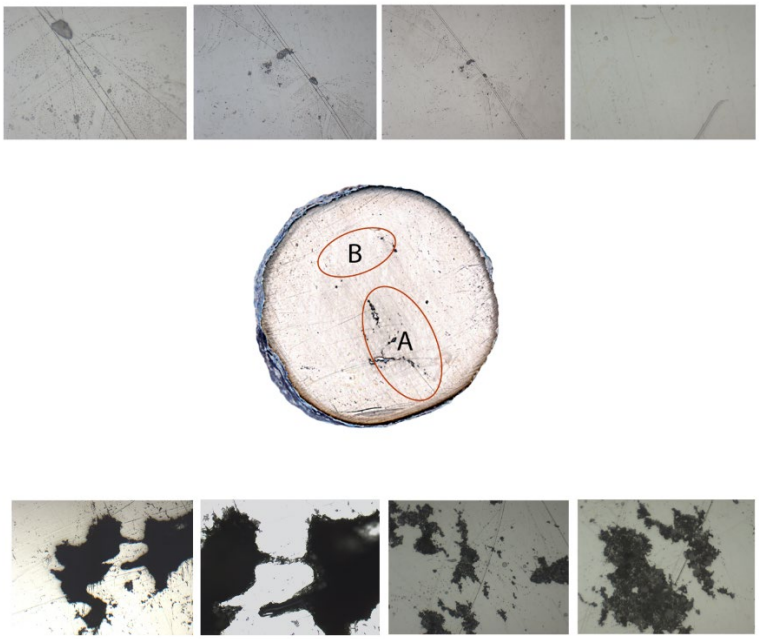

Figure 3.3-11 04-PI-TO Microscopy Photos before nital attack at different scale of the zone B(Top) and zone A (Bottom)

The two different areas of *04-PI-TO* after nital attack:

- **A**: α + Cementite
- **B**: Pearlite + Cementite

As it can be seen in the image **zone B** have clear lamellae structures of Pearlite.

The formation of **spheroidal pearlite** can be ascribed to a slow cooling (normalization like) in the production process.

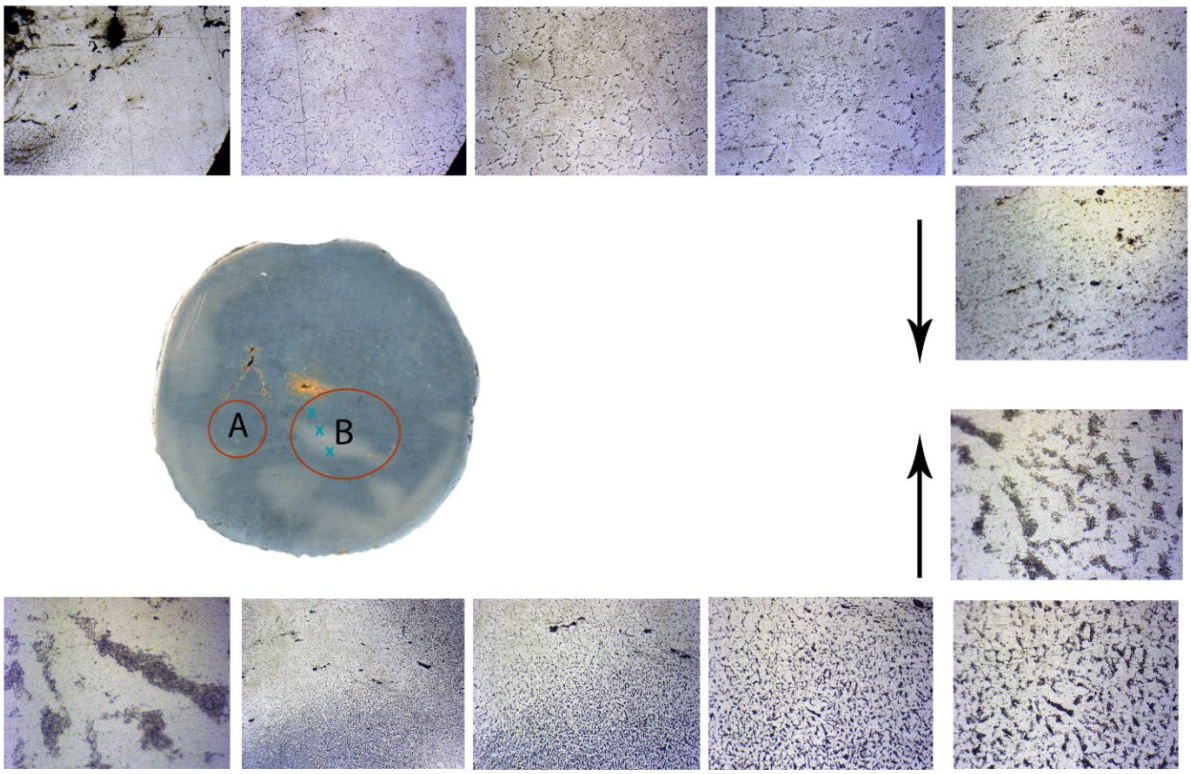

Figure 3.3-12 04-PI-TO Microscopy Photos after nital attack at different scale of the zone B(Top) and zone A (Bottom) after nital attack

It is interesting to note that in this kind of old bars the **amount of carbon varies a lot from section A to B**.

The reason could be ascribed to non-uniformities in the temperature while the operator gives the shape to the bar.

Considering Zone, A of 04-PI-TO the **small black dots** have been reconducted to **tertiary cementite** (Figure 3.3-14) since the carbon percentage in this zone is quite low and the slow cooling rates. (Figure 3.3-13)

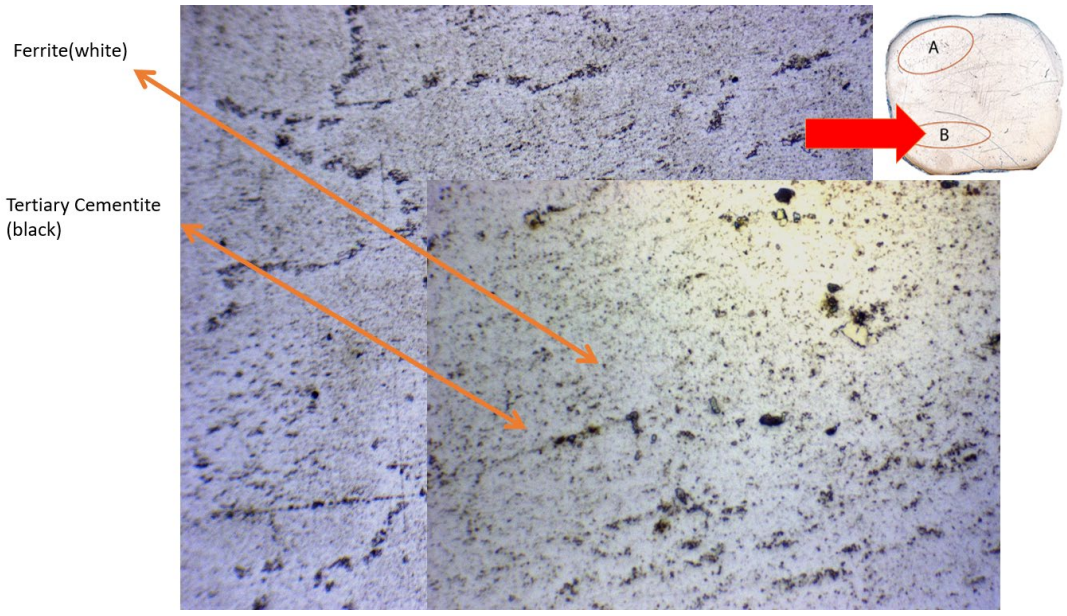

Figure 3.3-13 Zone A of 04-PI-TO after nital attack: Tertiary cementite(black) in ferrite(white) matrix

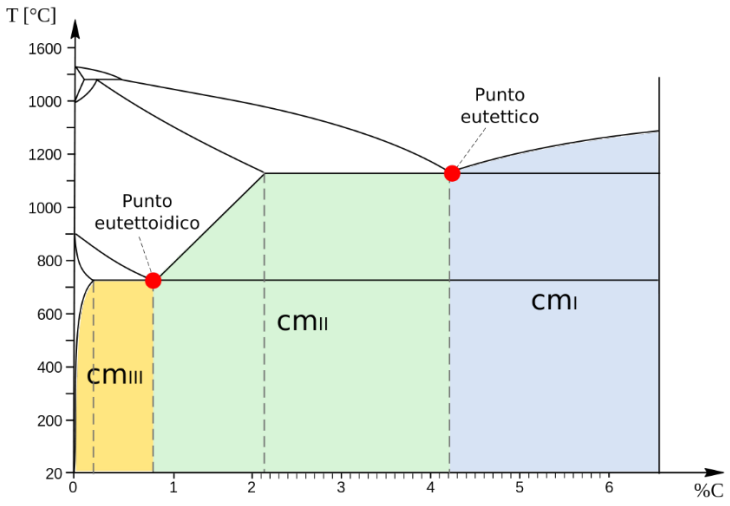

Figure 3.3-14 Tertiary Cementite representation (orange section) (22)

Looking at zone B of 04-PI-TO (Figure 3.3-15) it is possible to see a kind of **spheroidal pearlite** caused by the slow cooling in the manufacturing process.

The matrix is made of ferrite (low carbon percentage zone).

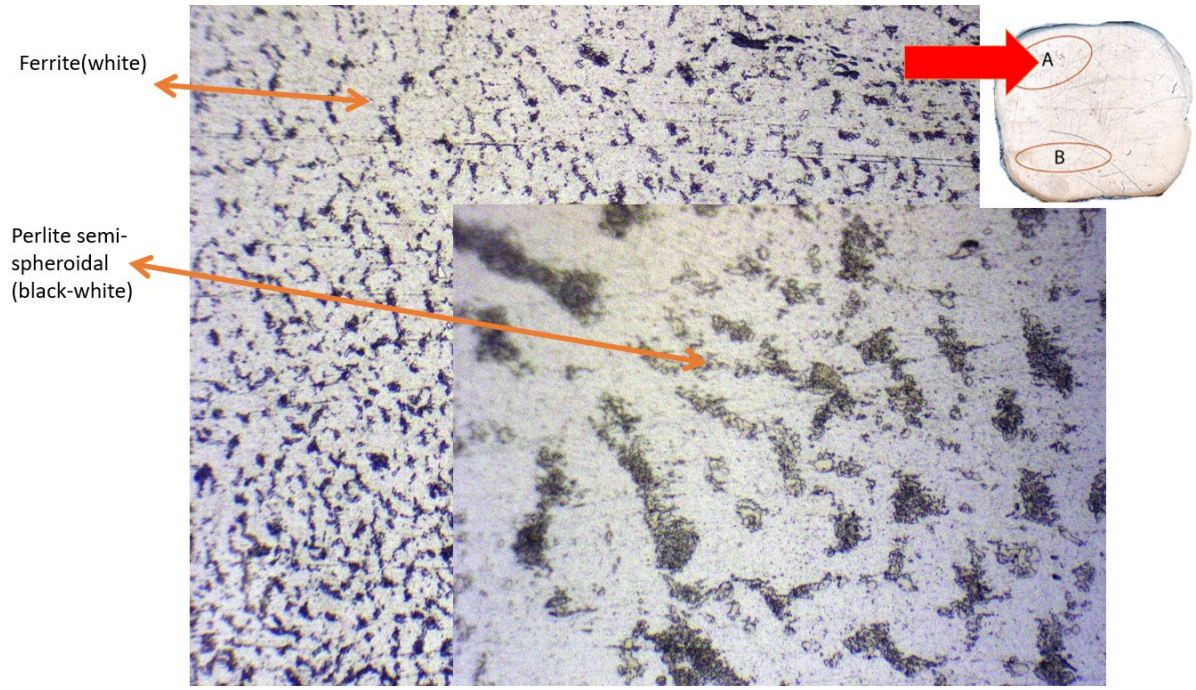

Figure 3.3-15 Zone B after nital attack of 04-PI-TO: ferrite(white) and semi-spheroidal pearlite(black)

3.4 Micro Hardness Analysis

The hardness analysis has been carried with **sample 04-PI-TO** after a nital attack in 5 different points distant 100µm between each other of the B zone of the metal with a Vickers Hardness Testing machine. (Figure 3.4-1)

Figure 3.4-1 **Vickers Hardness testing Machine in the Lab**

Furthermore, **a short statistical analysis** of the 25 total measurements(**Table 3.4-1**) was conducted to find the **average and standard deviation** values of the material's hardness *depending on the concentration of Fe3C.*

The results can be seen in the table below.

Table 3.4-1 Hardness dependency on the Fe3C concentration. (brief *Statistical Analysis*)

04-PI-TO	**High** Density of Fe3C	**Medium** Density of Fe3C	**Low** Density of Fe3C
1	138.2	110.9	112
2	140.9	114.8	114.1
3	131.4	114.1	104.3
4	118	106.5	101.4
5	121	106.4	124.2
AVARAGE	129.9	110.54	111.2
STANDARD DEVIATION	9.088014084	3.58920604	8.021221852

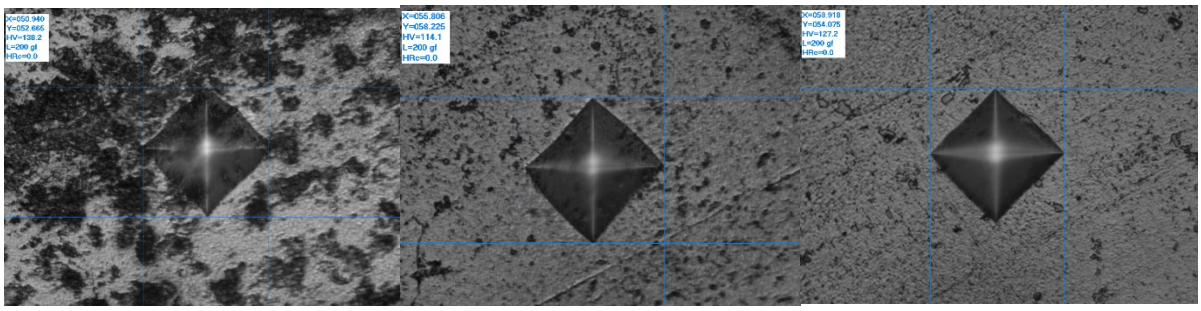

Figure 3.4-2 From the left to the right: High, Medium, Low percentage of Cementite (Fe3C)

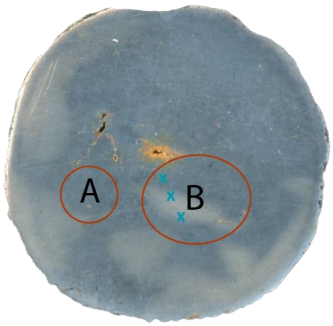

Figure 3.4-3 Specimen 04-PI-TO. The point where hardness was measured are depicted by x

in the B zone. The points are *distant 3÷4 times* the size of the imprint.

The results obtained are in line with material science *since the zones with a greater amount of Fe3C evidence the highest hardness* (greater amount of C*)* while the **<u>zones poor of Fe3C depict a lower hardness</u>**. (Figure 3.4-4)

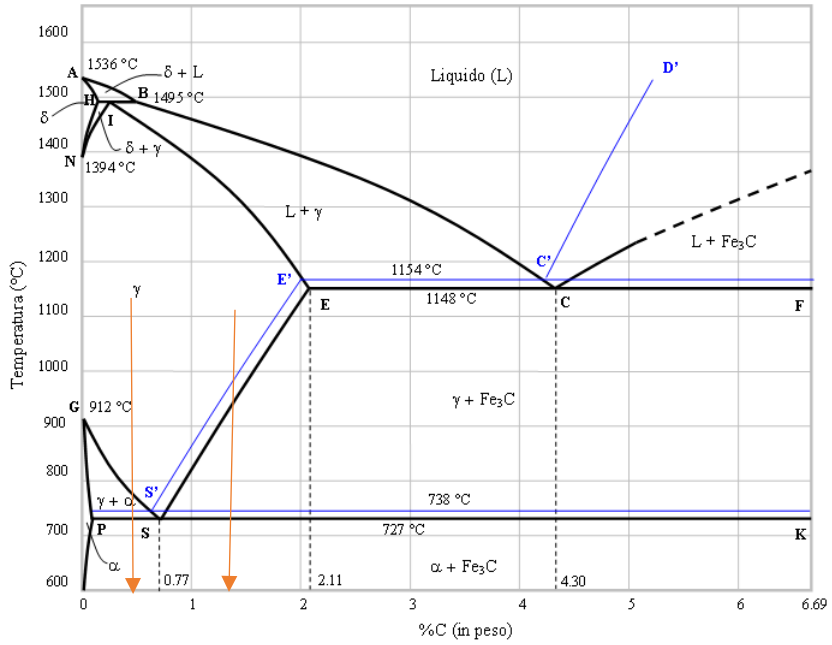

Figure 3.4-4 Diagram Fe-C. The composition of our metal can be seen at the end of the transformations (2 yellow arrows) depending on the carbon percentage of the specific zone.

3.5 Analysis of inclusion through Acid Second Phase Extraction

3.5.1 Introduction

During this experiment, a carbon steel specimen (**civil engineering steel**) has been dissolved in acid to **detect non-metallic inclusions** in order to investigate the possible *production process* of the latter.

The chemical recipe of the experiment comes from the "*Standard Test Method for Acid-Insoluble Content of Copper and Iron Powders*" (23) and an extract it is attached down below.

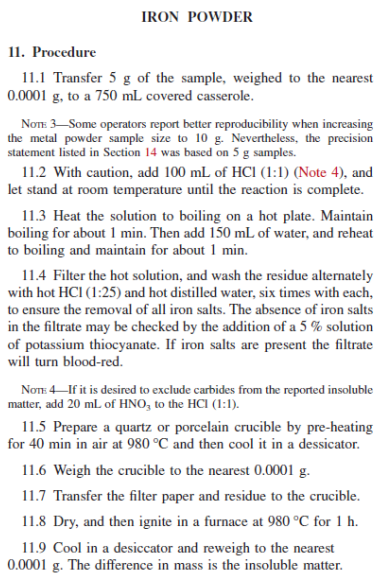

IRON POWDER

11. Procedure

11.1 Transfer 5 g of the sample, weighed to the nearest 0.0001 g, to a 750 mL covered casserole.

NOTE 3—Some operators report better reproducibility when increasing the metal powder sample size to 10 g. Nevertheless, the precision statement listed in Section 14 was based on 5 g samples.

11.2 With caution, add 100 mL of HCl (1:1) (Note 4), and let stand at room temperature until the reaction is complete.

11.3 Heat the solution to boiling on a hot plate. Maintain boiling for about 1 min. Then add 150 mL of water, and reheat to boiling and maintain for about 1 min.

11.4 Filter the hot solution, and wash the residue alternately with hot HCl (1:25) and hot distilled water, six times with each, to ensure the removal of all iron salts. The absence of iron salts in the filtrate may be checked by the addition of a 5 % solution of potassium thiocyanate. If iron salts are present the filtrate will turn blood-red.

NOTE 4—If it is desired to exclude carbides from the reported insoluble matter, add 20 mL of HNO_3 to the HCl (1:1).

11.5 Prepare a quartz or porcelain crucible by pre-heating for 40 min in air at 980 °C and then cool it in a dessicator.

11.6 Weigh the crucible to the nearest 0.0001 g.

11.7 Transfer the filter paper and residue to the crucible.

11.8 Dry, and then ignite in a furnace at 980 °C for 1 h.

11.9 Cool in a desiccator and reweigh to the nearest 0.0001 g. The difference in mass is the insoluble matter.

Figure 3.5-1 Extract Of "*Standard Test Method for Acid-Insoluble Content of Copper and Iron Powders*".

3.5.2 Process Description

To **accelerate the dissolution** process of the metal our specimen has been machined so to obtain **small chips**.

In addition, the chips have been faced on a lathe so to obtain a much **smaller surface area** which is exposed to the extracting solution leading to a considerably faster reaction.

(**Figure 3.5-2**: **Chips of the specimens inside a 1000 ml flask.**)

Figure 3.5-2: **Chips of the specimens inside a 1000 ml flask.**

The total **weight** of metal chips was measured before and after extraction to enable the determination of the **dissolution rate**. A weight of 0.059g has been measured with a super precise **balance**. (**Figure 3.5-3** Balance to measure the chips and the filter's weight before and after the extraction of the second phases.)

Figure 3.5-3 Balance to measure the chips and the filter's weight before and after the extraction of the second phases.

In the second place, **two** beakers with respectively HCL **(1:1)** and HCL **(1:25)** have been filled up with distilled water and HCL in the respective proportions. (**Figure 3.5-4** *On the left* Main Ingredients for the)

Moreover, both the HCL beakers have been heated to an average boiling temperature of T=100°C with a **magnetic stirrer** to help the mixing process and heat the liquids.

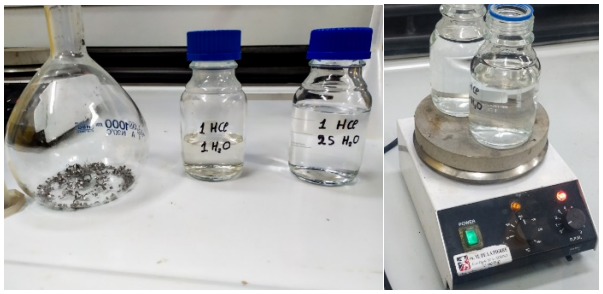

Figure 3.5-4 *On the left* Main Ingredients for the experiment. *On the right* the magnetic stirrer.

To start the experiment the **chips** in the 1000 mL flask have been **mixed** with the **HCL**(1:1) and heated to boiling temperature.

While boiling the **expected reaction** is:

Where **X** are the **inert inclusions** from the metallic matrix of our specimens.

$$X + Fe_{(l)} + 2HCl_{(l)} \rightarrow X + FeCl_{2(l)} + H_{2(g)} \qquad 3.5\text{-}1$$

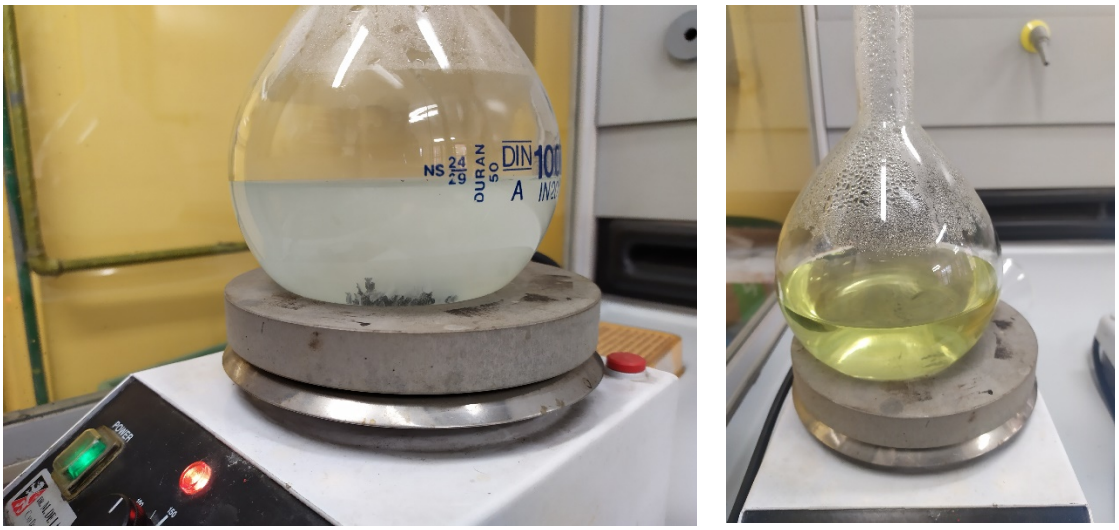

Figure 3.5-5 On the left has represented the start of the reaction. On the right end of the reaction with FeCl2(l) in *green*.

After most of the metal chips dissolved a **paper filter** has been adopted to catch the inclusions in the liquid. (**Figure 3.5-6** Filter working with a vacuum pump connected to the lower)

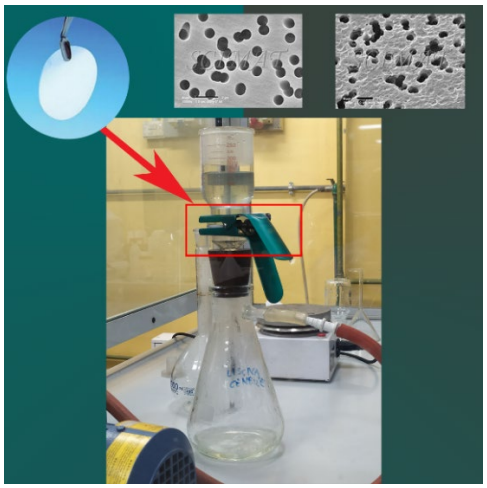

Figure 3.5-6 Filter working with a vacuum pump connected to the lower flask. Microscopy images adapted only for “illustrating purposes” and do not represent exactly the paper filter used (24).

In this phase, a **vacuum pump** has been used to facilitate the flow of the liquid into the flask. Few grams of the material were collected by the **filter** and they will be analyzed at the **SEM** electronic miscroscope in the next chapter.

3.5.3 SEM Analysis Introduction

A Scanning Electron Microscope (**SEM**) have been used to analyse the content of the filter. This type of microscope is really handy because it allows to expand the resolution range to around 10nm.

The SEM microscope works by shooting a high energy electron beam to the specimen and detecting the reflected signal with a sensor. (Figure 3.5-8)

The electrons get shoot from an electron gun thanks to a different of voltage from 2-100kV forced onto the system.

An electromagnetic lens then is idolized to converge the electron beam to the specimen in order to detect the signal.(Figure 3.5-7 Comparison between a traditional optical microscope and a SEM working principle (on the right). A series of magnetic lenses is used to converge the electron beam [25] (25),Figure 3.5-7)

By processing the signals coming from the specimen the PC can generate a black and white image of the surface.

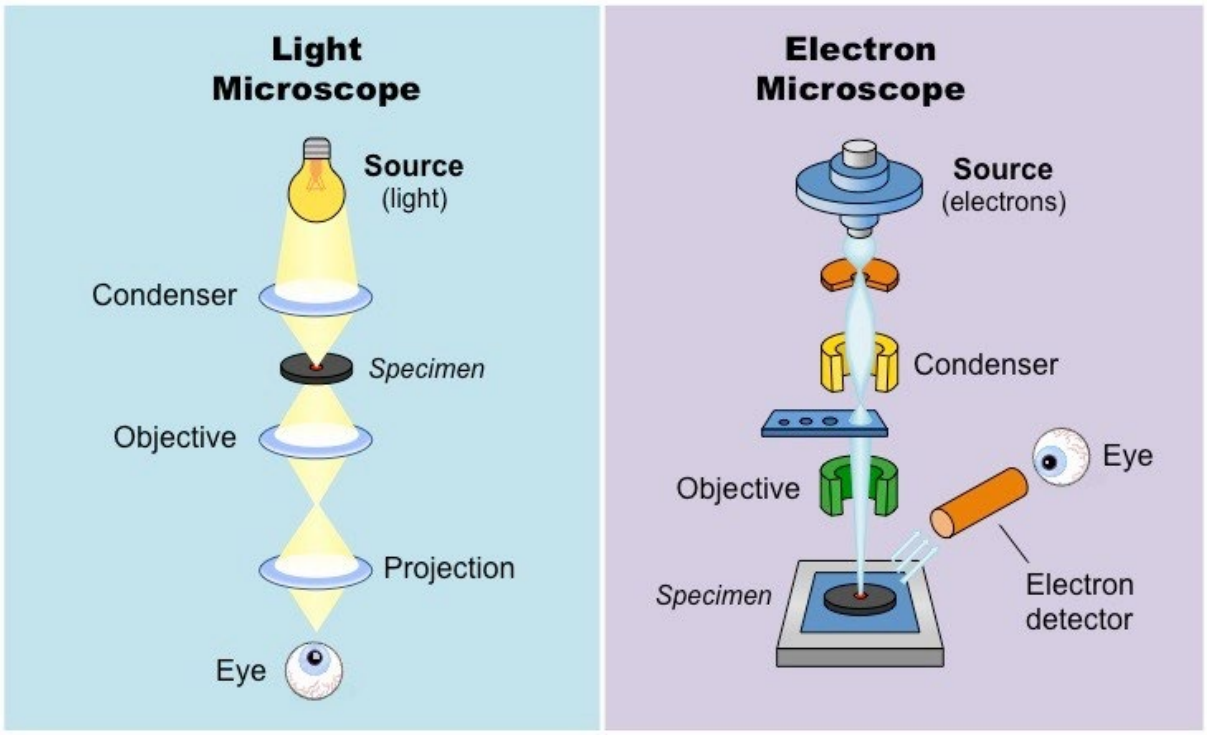

Figure 3.5-7 Comparison between a traditional optical microscope and a SEM working principle (on the right). A series of magnetic lenses is used to converge the electron beam (25)

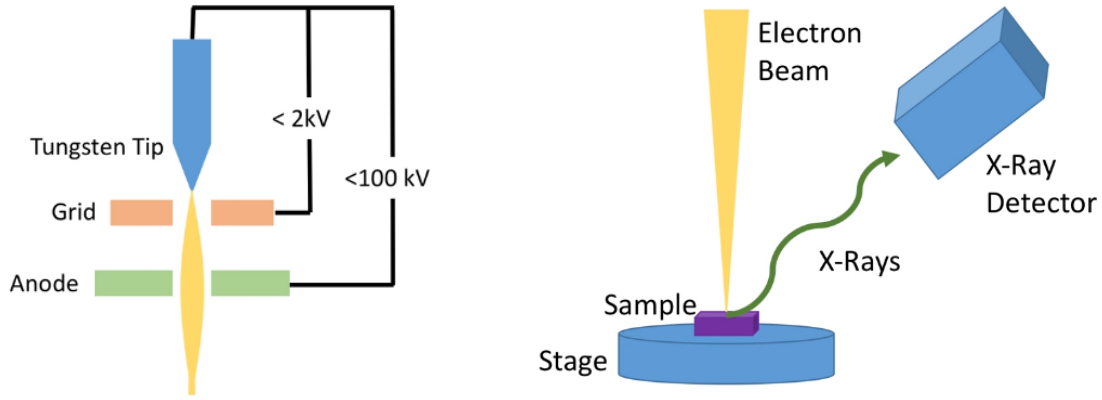

Figure 3.5-8 SEM working principle. Gun on the left and signal detection on the right (26)

3.5.4 SEM Analysis Results

The SEM showed clearly that our filter got **filled** with something. (**Figure 3.4-2**)

To be 100% sure that what has been detected is really an inclusion an EDS analysis will be performed in the next chapter.

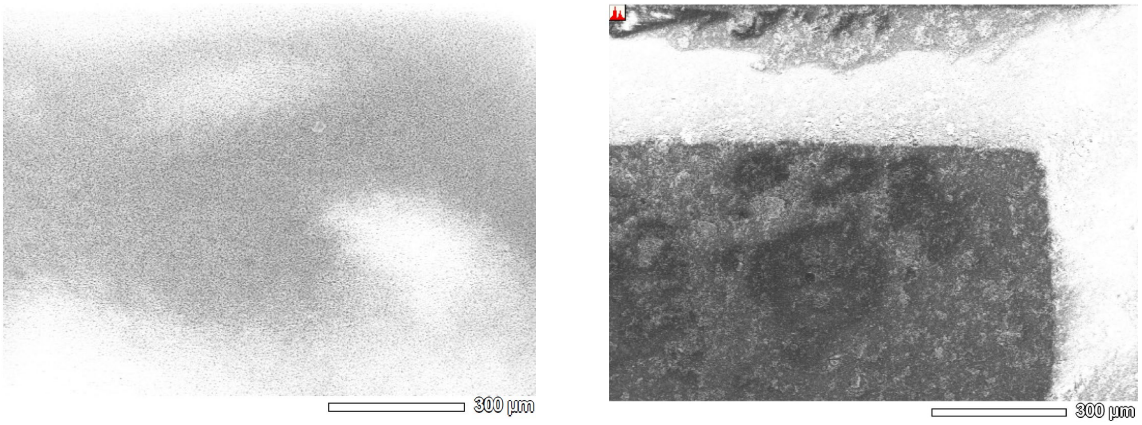

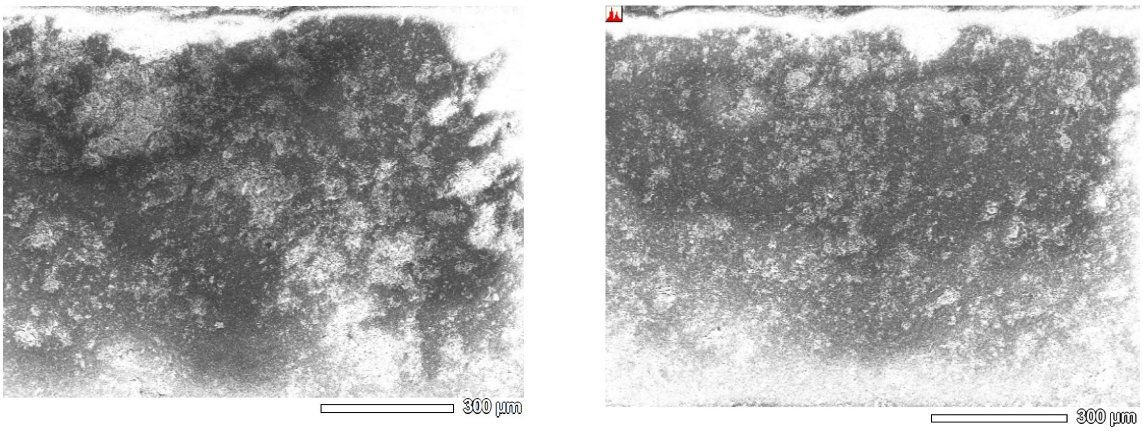

Figure 3.5-9: Top left new filter. The other pictures represent the used filter in 3 different spots.

3.5.5 EDS Analysis Working Principles

It is common that the SEM microscope comes equipped with EDS analysis capabilities.

To begin EDS operation an electron beam bombards the atoms of the specimen. The hit might excite an orbital electron at a high energy level as it can be seen in the Figure 3.5-10. (27)

At this point the electron may eject (back-scattered electron) leaving a vacancy in the inner shell. Consequently an electron from a lower energy orbit fills this gap releasing a radiation signal (secondary electron + x-ray) that it's detected by a sensor.()

Singe the energy gaps between the orbits of an atom are particular to every single element. Measurements of the radiation signal can lead to the knowledge of the elements present in the material.

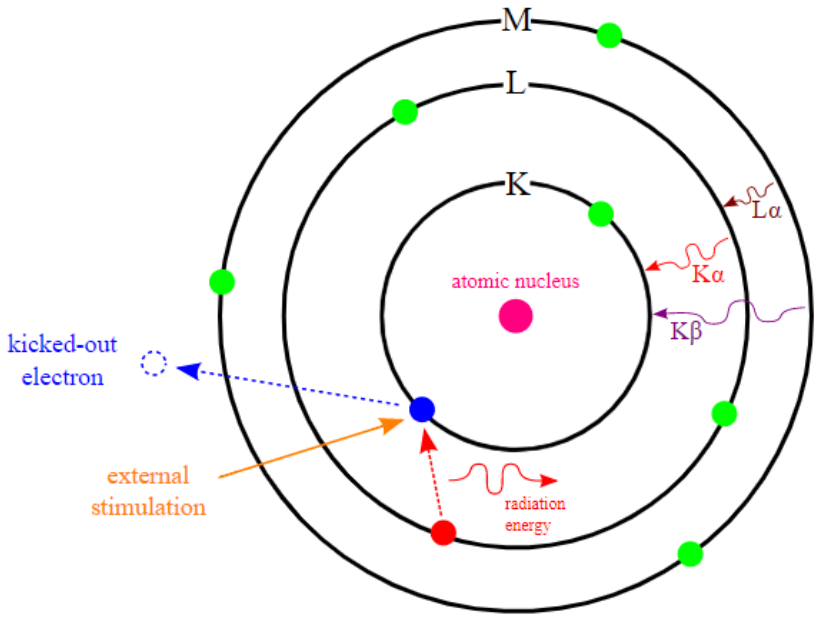

Figure 3.5-10 EDS Signal Emission Principle (27)

EDS is generally used for compositional mapping of a given sample.

Non only can relatively amount of each atom can be measured but the distribution of the atom in the sample can be mapped.

During SEM operations a high-energy electron beam hits the sample and some of these electrons

Further investigations revealed the chemical composition of the material residual inside the filter itself. (Figure 3.5-13)

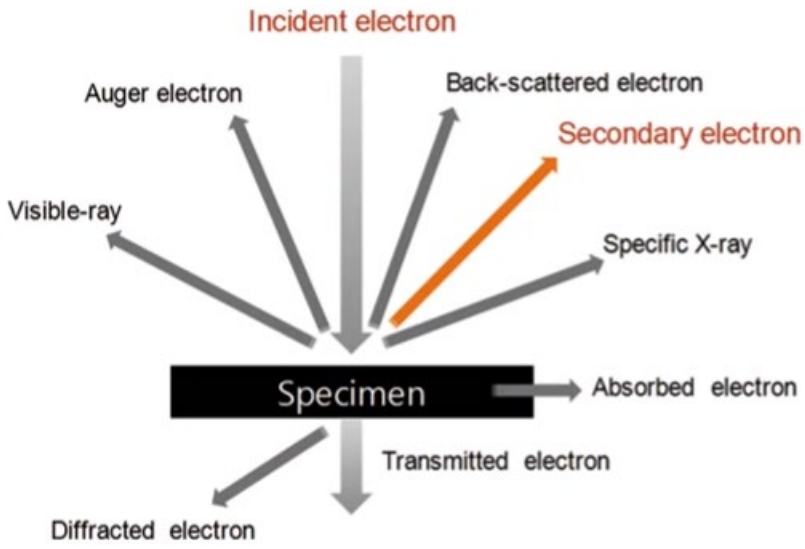

Figure 3.5-11 Schematic representation of the output radiation different contributions. (28)

3.5.6 EDS Analysis Results and Discussion

The signals acquired from the radiation caused by the incident electron beam topic of the previous chapter can now be represented on the relative quantity vs Energy content plot. Where the x axis is related to the Rydberg formula (1888):

$$E = \frac{h * c}{\lambda}[eV]$$

The various peaks all represent a particular element's relative percentage in the sample.
In order to remove the filters composition from the data and extract only the composition of the inclusions it is necessary to study first a new filter (Figure 3.5-12) and then a filter filled with possible inclusions(Figure 3.5-13).

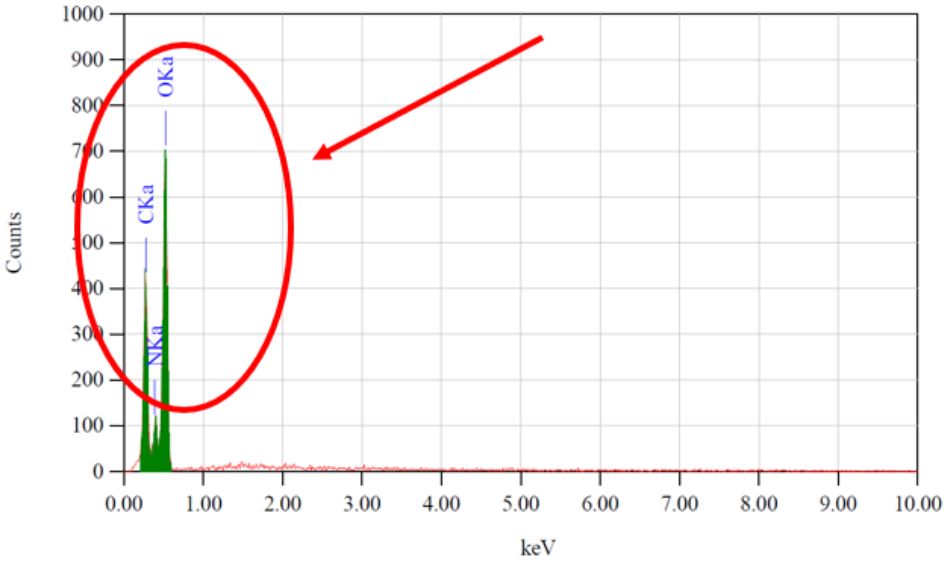

Figure 3.5-12: SEM quantitative analysis of new filter. The arrow shows the empty filter's actual composition.

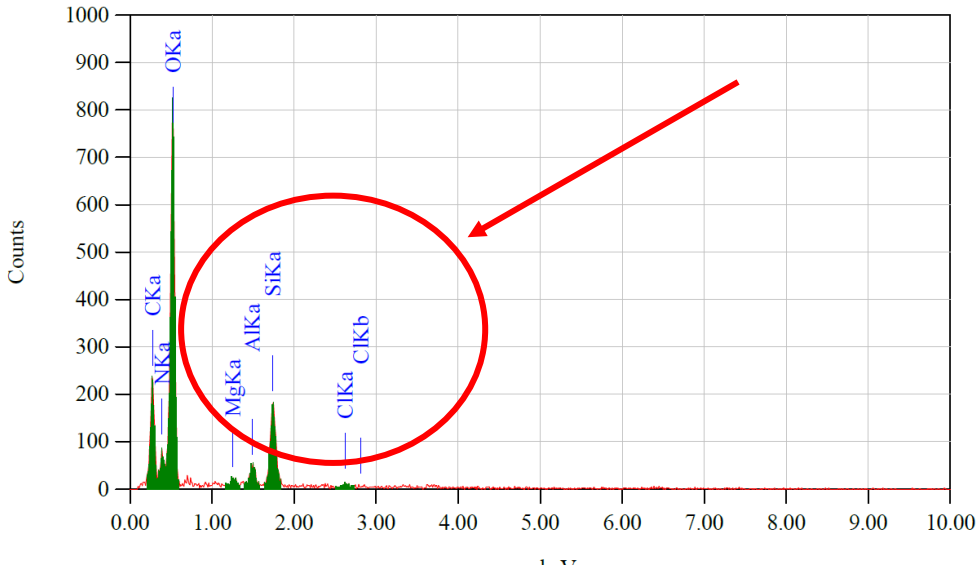

Figure 3.5-13 SEM quantitative analysis of the chemical composition of the filter of our filter with inclusion's composition (red arrow).

ZAF Method Standardless Quantitative Analysis
Fitting Coefficient : 0.1252

Element	(keV)	Mass%	Sigma	Atom%	Compound	Mass%	Cation	K
C K	0.277	20.32	0.35	25.59				11.8338
N K	0.392	10.70	0.68	11.55				15.6072
O K	0.525	63.15	1.01	59.70				66.1309
Mg K	1.253	0.39	0.06	0.24				0.3056
Al K	1.486	1.01	0.09	0.57				1.0866
Si K	1.739	4.18	0.17	2.25				4.7000
Cl K	2.621	0.24	0.05	0.10				0.3358
Total		100.00		100.00				

Figure 3.5-14 Quantitative EDS analysis

Inspecting the chemical composition of the filled filter the more relevant peaks related to the possible inclusions are: **"Magnesium**, **Aluminium, Silicon and Chlore**". (Figure 3.5-14)
It is worth note that those elements are not present in new filters (**Figure 3.5-12**) and that are the most common second phases in steel metals as discussed in the *1st Chapter of this thesis*.
The new filters had Oxygen, Nitrogen, Carbon, and those elements show higher peaks in the used filters since they are present both in the new filters and in the oxides of Magnesium, Aluminium and Silicon. Hence those oxide may have been present in the initial iron ore.
The relatively high amount of Magnesium and Aluminium oxides suggest that the examined tie-rod was produced through the direct process.
However due to the low number of slag analyses this remains good hypothesis but without a robust statistical evidence.

3.6 Conclusions

This chapter tried to find the production process of a 17th century iron tie-rod from a masonry building in Turin. The metallographic analysis showed clear non homogeneities in the carbon percentage and inclusion distribution from different zones of the same cross section and even from cross section to cross section. This suggests the presence of a temperature gradient in the

final forging process. On the other hand, the composition of the inclusions investigated though the EDS analysis presented oxides typical of the bloomery of direct steelmaking process.

Moreover, the microstructure found by optical metallurgy where mainly ferrite, cementite, and pearlite. All those microstructures suggest a slow cooling.

Finally of all the scientific evidence found in the previous sub-chapters we could hypnotize that the steelmaking process was bloomery, the piece was slow cooled with a temperature gradient in the final forming.

4 Analysis of An XVI Sword

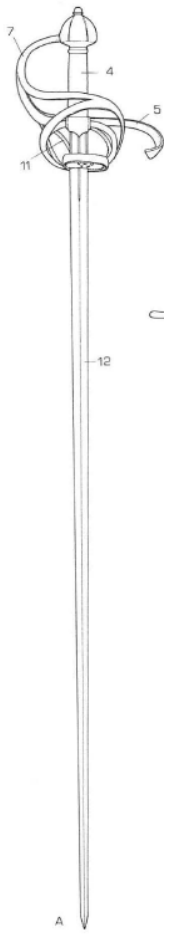

4.1 Introduction

In this chapter will be devote to the analysis of the microstructure of an **XVI Century Italian sword** (Figure 4.1-1) kindly offered to **Polito** by the *Museo delle Armi "Luigi Marzoli"*.

Swords can be located temporally with extreme precision thanks their aesthetic features and morphology.

Thus, they can give remarkable insight about the technological and economical level of a particular civilization.

Many of the production methods of swords of this kind were a secret kept from master blacksmith by generations.

By metallographic studies it is now able to unveil some of these secrets such as thermal treatments and production systems of that time.

Furthermore studying the microstructure at a microscope, it is possible to estimate the carbon

percentage and the manufacturing process.

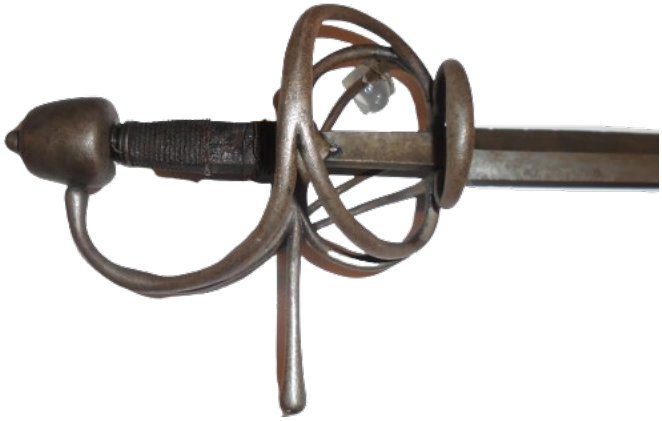

Figure 4.1-1 The sword of the L. Marzoli Museum of Brescia examined in this chapter, listed as G59.

4.2 The G59 Sword

The Figure 4.1-1 shows the examined Italian sword of the XVI century most likelly forged in **Belluno,Italy**.

In fact, Belluno in that period was the main production area for some of the most popular swords in Italy. (29) This specific **rapier** is part of the "**L. Marzoli**" collection from the Mouseoum of Brescia and it's catalogue listing number is **G59**.Unfortunatelly some of the length close to the tip didn't come to our days.Due to the bad state of conservation the museum granted the permission required to start studying it. **G59** is estimated to be an expensive accessory for noble men in the **XVI century** in Italy. (30)

In fact the description of a similar rapier ((31),Figure 4.2-3) conserved at Metropolitan museum of Art in New York states: "From the early sixteenth century onward, the practice of wearing a sword or rapier with civilian dress made duels between unarmored opponents more

common. Lacking the armor or shield worn in battle, combatants had to block or parry an attack by other means.(…) During the sixteenth and seventeenth centuries, distinct schools of fencing developed rapidly in Italy, France, Germany, and Spain.” (32)

As it can be seen in **Figure 4.2-1** differents rapier sword blacksmiths all around the european area used slidly different styles ,e.g for the quillion to match, the taste of thieir costumers needs and social class appartenance.

Figure 4.2-1 A selection of Italian style rapiers from the left to the right; Milan, c. 1620; Naples 1610-20:London;c. 1580-90;Milan,c1620 (33)

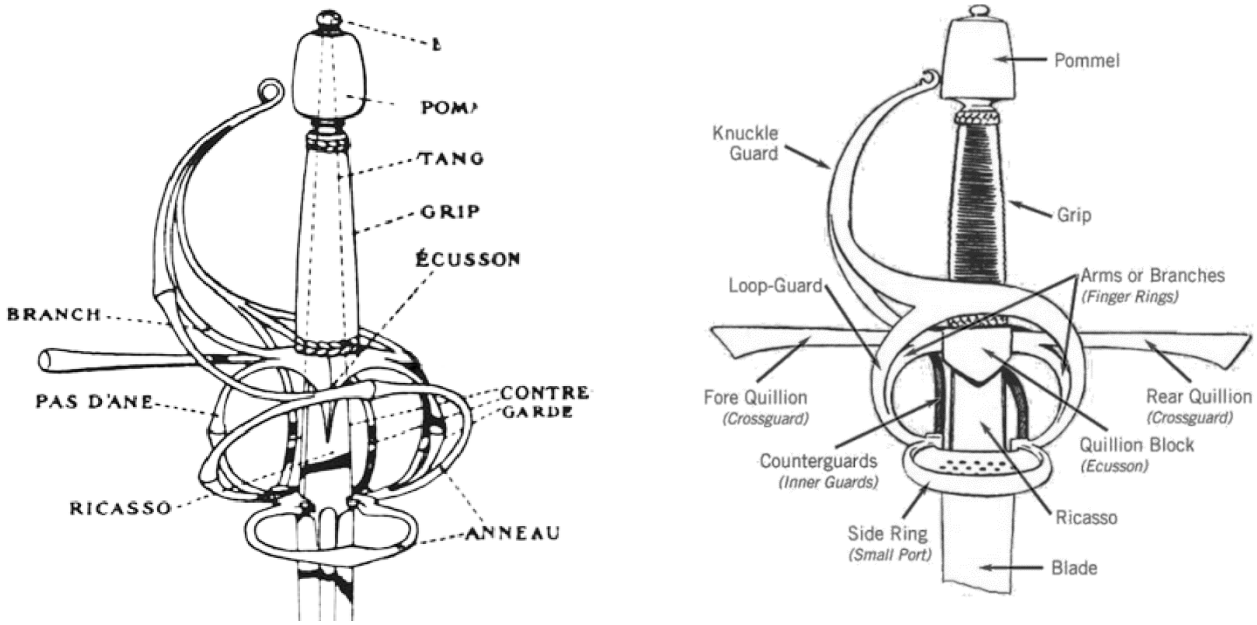

Figure 4.2-2 Nomenclature of each part of the rapier in French on the left and in English on the right (33)

Figure 4.2-3 Similar Sword conserved at the Met Fifth Avenue in Gallery 376 of the Metropolitan Museum of Arts of New York (32)

4.3 Sampling

The sword have been collected and cold cutted in locus at the museum of Brescia according to the scheme in the **Figure 4.3-1.**

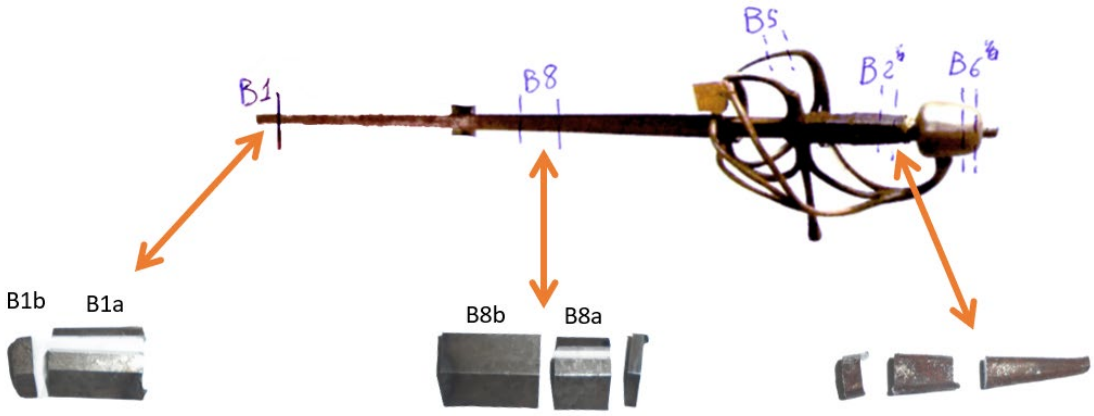

Figure 4.3-1 The samples obtained from the G59 sword. The sample B1 have been sectioned

in 2 parts B1b and B1a.B1b is the transversal while B1a is the longitudinal cross section. The same can be said for the B8 sections.

The applied type of cut is referred as *cold sawing* and it is advisable for the kind of metallographic analysis that will be performed in the next chapters since there is no risk in changing the microstructures due to an increase in temperature.

Moreover B1a,B1b, B8a, B8b have been supposed to metallographical analysis.(**Figure 4.3-1)**

Howerver during such analysis B8b showed a very peculiar microstructure so it got an extra micro hardness analysis for further investigations.

Figure 4.3-2 Photo of the Swords before and after the cuts

4.4 Specimen Preparation

To examinate the microstructures of the sword followed a similar procedure as the of the tie-rods discussed in the 1st *Chapter* although with a slightly different nital etching%.

To facilitate gripping during the grinding the specimen have been **cold embedded** in a resin. (**Figure 4.4-1**)

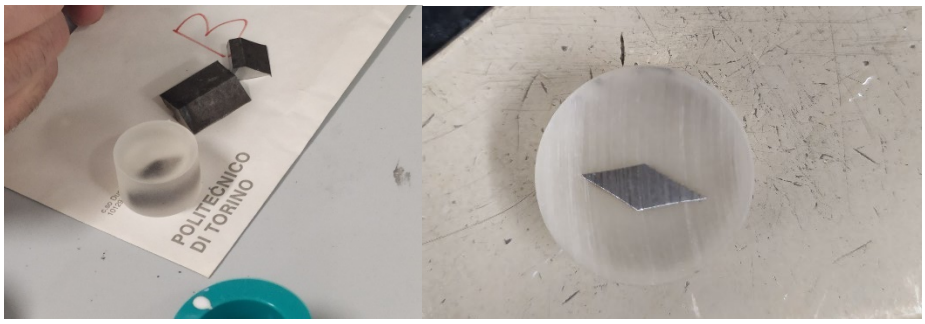

Figure 4.4-1 **Embedded sample example.**

Finally, all 4 embedded sections of the sword were obtained, ready for the next analysis.

4.5 Metallographic Analysis

4.5.1 The Blade "Tip" Section

The Figure 4.5-1 show the etched transversal section of the blade 'tip'. As mentioned before real blade end got lost and did not arrive to our days so we will call 'tip' what is left of it.

The **B1b** transversal section specimen after nital attack shows a mainly **Acicular Martensitic (black aciculae)** with some **Bainitic (white aciculae)** microstructure from the 'self-tempering' process with areas of higher and lower carbon concentration as it can be seen in Figure 4.5-1.

The presence of martensite is to be ascribed mainly to the quenching procedure in the production of the sword.

In fact, **Martensite** formation require a diffusionless transformation ("instant" [≈ms] =no time dependency) and quenching is quick enough to be considered diffusionless.

All the possible combinations of phases that are obtainable from a quenching heat treatment

can be seen from the CCT or TT diagrams. (Figure 4.5-2)

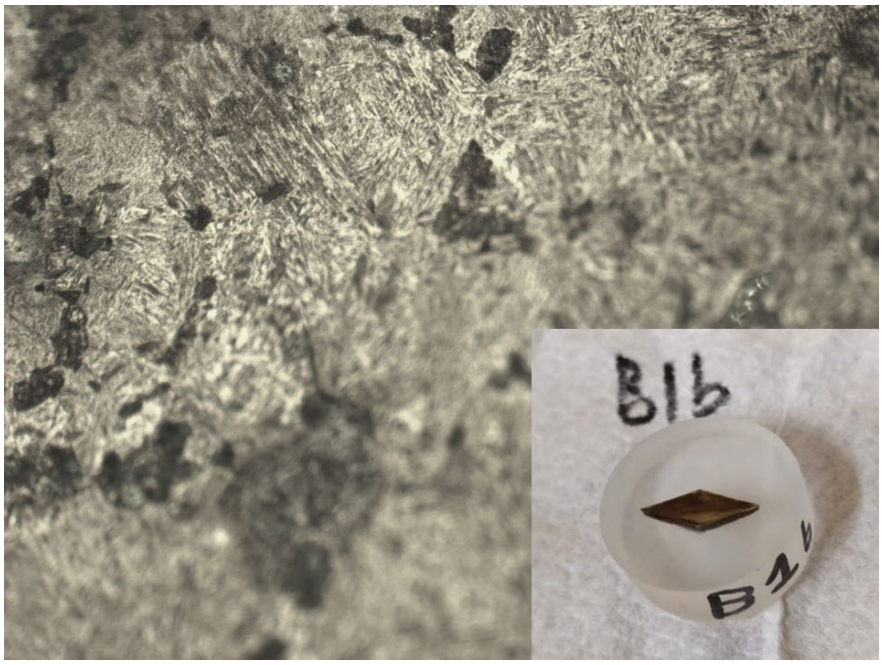

Figure 4.5-1 01-PI-TO Microscopy Photos of the zone B1b after a nital attack shows clear aciculae structures attributable to Martensite and Bainite. The image also shows the presence of some black insulae that could be inclusions.

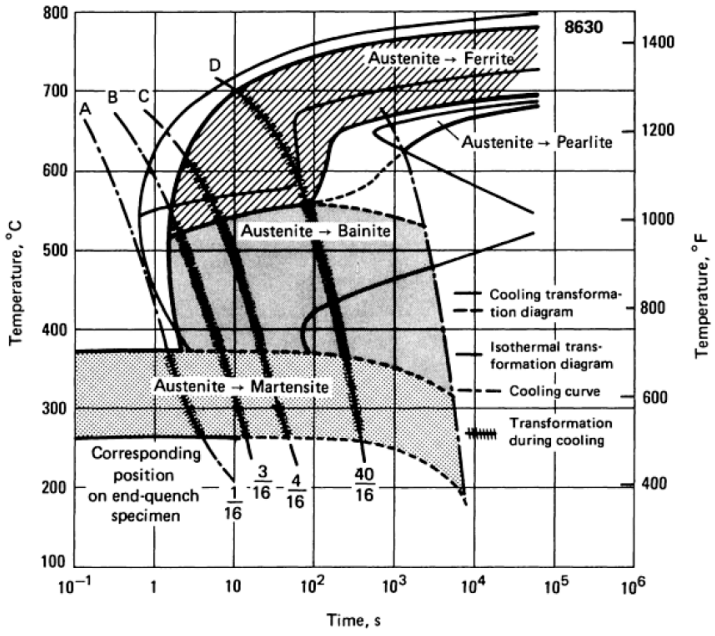

Figure 4.5-2 Illustrating Example of a typical quenching CCT diagram. (17)

The **B1a** longitudinal section after nital attack shows the same microstructure of **B1b.** (the cut

plane of B1b is a 90° from B1a).

Indeed the section rich of carbon (black areas) outlines the direction of the forging process as it can be depicted by the red arrows in the image .

Figure 4.5-3 01-PI-TO Microscopy Photo of B8b longitudinal cut section microstructure. The microstructures are Martensite and Bainite because B1b is at 90° of B1a.

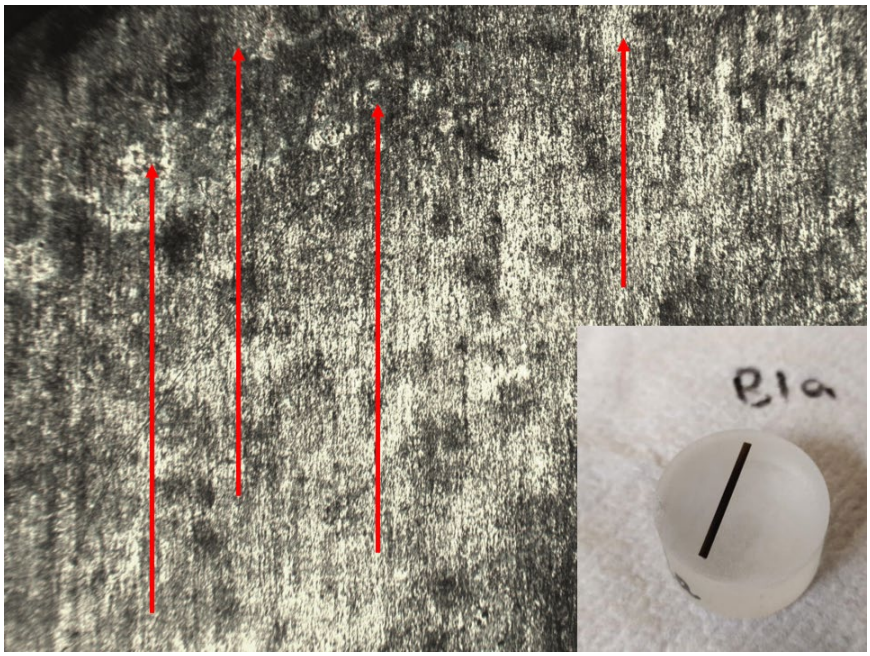

Figure 4.5-4 Metallography Photo of B1a.Directionality is shown by the red arrows.

Moreover, the martensite takes a lath shape because of the sword carbon percentage falls in between 0<%C<0.60.(Figure 4.5-5)

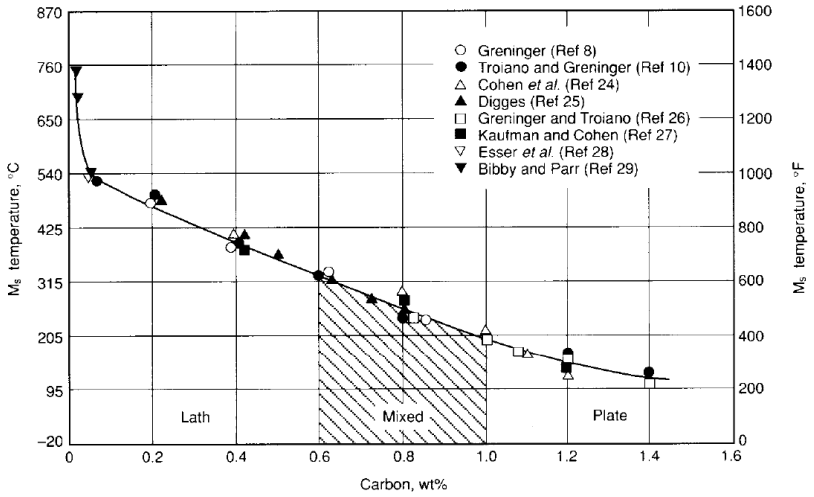

Figure 4.5-5 Martensite shape as function of the carbon percentage. (34)

In sight of the found microstructures we can hypotheses that the blade have been completely austenitized(T>$A_3 = 920°C$) at least towards the tip and then quenched rapidly to produce Martensite.

Afterwards the sword may have been extracted from the quenching liquid to be left self-tempering at room temperature producing bainite in the process.

4.5.2 The Blade "Middle" Section

The **B8b** specimen after nital attack (Figure 4.5-6) shows a microstructure that seems to be of prevalently tempered martensite with some islands of $\propto (ferrire) + Fe_3C$ surprisingly (Figure 4.5-7).

The presence of the latter can be caused to not reaching the complete austenitization

temperature (A_3) homogeneously along the sword, then **hammering** and finally **quenching the ferrite + Cementite**.

In fact, these really ordinate shapes come out from the transversal section of the sward as if they are residuals of a four directional hammering operation that lead to the final rhomboidal section of the sword right after the extraction from the quenching liquid.

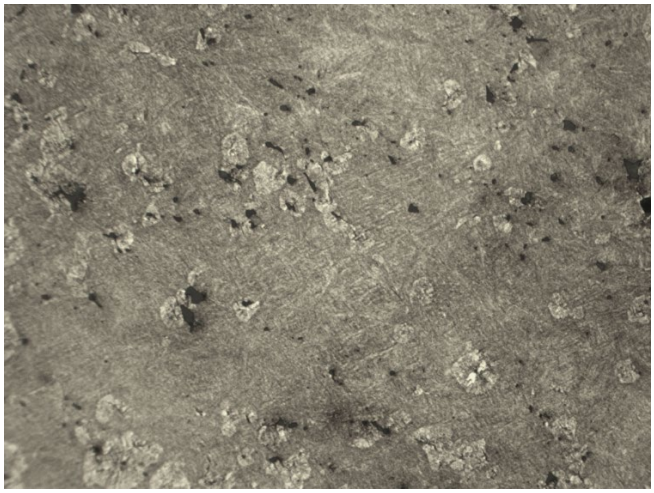

Figure 4.5-6 Microscopy Photo@20x1 of B8b transversal cut section microstructure. The matrix is martensitic while the white sort of clusters is ferritic+cementitic.

Figure 4.5-7 Microscopy Photo@100x1 of B8b transversal cut section microstructure. This sort of ordinate rectangular shapes could be referred to ferrite(white) and cementite(black)

Probably since the *swordsmiths* heat up the blade holding it partially by the pinners and check the temperature merely by the colour of the metal and mistakenly, they did not reach A_3 homogeneously along all parts of the sword.

Hence the areas (at high carbon percentage) that reached A_3 austenitized and became martensite after quenching while the zones(low carbon percentage) that did not reach A_3 remained ferrite and cementite.

However, the formation of a microstructure of ferrite+cementite as in the Figure 4.5-7 may have not be done willingly by the manufacturers because this combination leads to a much lower hardness where especially in this kind of weapon the hardness can make the difference between life or death.

4.5.3 Comparison between Tie-rod Steel and Sword Microstructures

The metallographic sections before the nital attack show some small dots that could be inclusions. (Figure 4.5-8)

The distributions of such dots in the sword seems more homogeneous, with a lower density of population and with smaller dots compared to the tie rod steel analysed in *Chapter 2*.

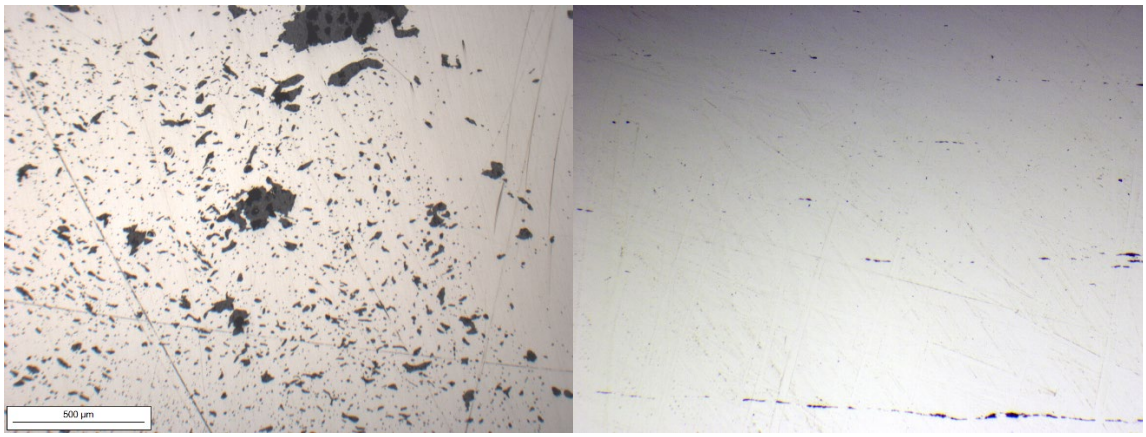

Figure 4.5-8 Rod Steel cross section on the left and G59 sword cross section to the right.

In fact the during the production process of these materials they both need to be hammered to "squeeze" away the inclusions (black dots).

The difference is that the sword being a higher quality product got hammered more until much of the impurities got ripped away from the metallic matrix.

Probably the inclusions had origin in the

4.6 Micro Hardness Analysis of the B8b Mysterious Structure

To investigate better the nature of the microstructure of the sword mean section a series of **micro hardness tests** have been performed with a similar procedure to the one performed with the **chain** subject of the first chapter of this thesis.

Due to small irregularities in the planarity of the surface caused by cold embedding and grinding it was necessary to use a **clamp** (**Figure 4.6-1**) to create a smooth plane.

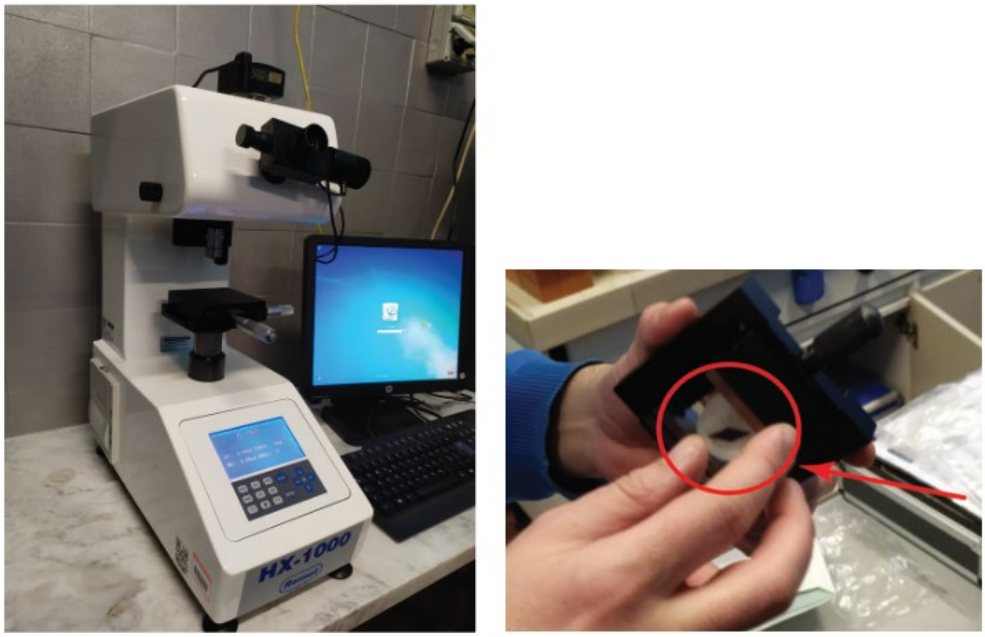

Figure 4.6-1 Clamp for the Specimen on the right and microhardness machine on the left.

A **statistical analysis** performed on **B8b** with micro hardness measurement machine revealed the hardness to be **380.7HV** on average between the short and long diagonals. (**Table 4.6-1**)

Table 4.6-1 Short statistical analysis of B8b on the rhomboidal section

Zona Mysterious Spada	Short Diagonal	Long Diagonal
1	362.9	418.2
2	442.6	504.4
3	427.9	295.6
4	422.1	232.2
5	425	211.8
6	455	204
7	401.7	476.5
8	345.5	460.8
9	320.6	445.9
AVARAGE	400.3666667	361.0444444
STANDARD DEVIATION	43.94981987	116.4855366
Total AVARAGE	380.7055556	

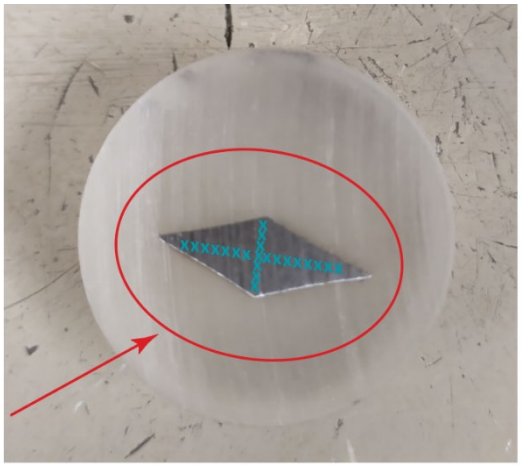

A **statistical analysis** performed on the data acquired from the micro hardness measurement machine revealed the hardness of the **Ferrite+Cementite area** to be **249.44HV**.

(**Table 4.6-3**)

Table 4.6-2 Short statistical analysis of the Ferrite+Cementite area of B8b

Ferrite+Cementite Spada	
1	282.9
2	268.8
3	251.5
4	232.2
5	211.8
AVARAGE	249.44
STANDARD DEVIATION	25.34802556

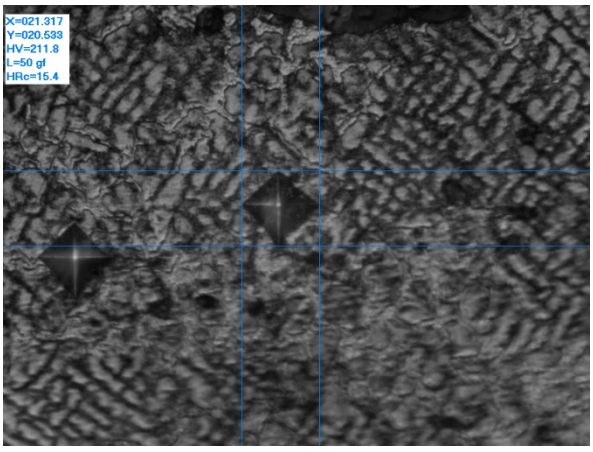

A **statistical analysis** performed on the data acquired from the micro hardness measurement machine revealed the hardness of the **Martensitic area** to be **560.44HV**. (**Table 4.6-3**)

The fact that is this result in hardness is the highest measured so far is congruent with Martensitic microstructure.

Table 4.6-3 Short statistical analysis of the Martensitic area of the sword (B8b)

Martensite Spada	
1	540
2	553
3	556
4	548
5	565
6	570
7	565
8	567
9	580
AVARAGE	560.4444444
STANDARD DEVIATION	11.57690336

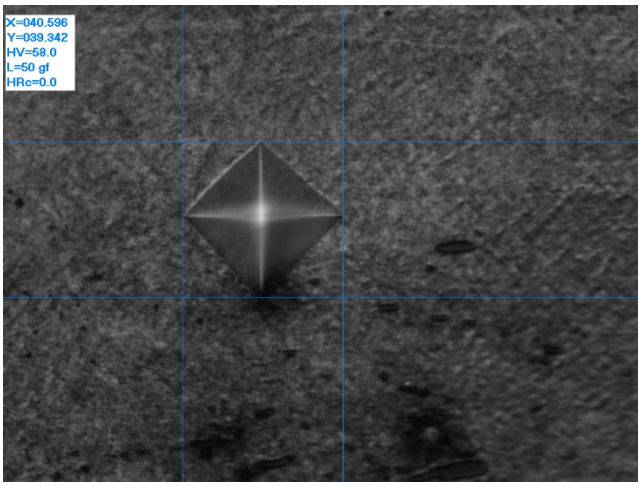

4.7 Discussion and Experimental Conclusions

In sight of the found microstructures we can hypotheses that the blade towards the tip (B1) have been completely austenitized(T>$A_3 = 920°C$) , then quenched rapidly to produce Martensite, afterwards extracted from the quenching media before thy where completely cold e left self-temper due to the heat conduction mainly from the tang.

The hardness of the aciculae structure analysed was of around 560HV, so it is reasonable to say that it is Martensite + Bainite from tempering.

On the other hand, the middle of the blade(B8) did not even reach complete austenitization but only partial austenitization.

This hypothesis could be justified by the measured hardness of the ferritic+Cementitic areas to be of 249 HV.

As a result, the middle of the blade could have a structure of ferrite and cementite in a martensite matrix.

A hypothesis on the cause of this interesting ordinate square shapes observed in the ferritic + cementite clusters could be that it generated during the hammering the sword, the manufacturers did to give the rhomboidal shape of the transversal cross section.

Furthermore, we can expect an increase in hardness from the tang to the tip thanks to the fact that the closer to the tip of the blade will have the highest concentration of martensite.

The waiting time of the blade in the quenching water has to be accurately thought upon to get the best compromise between hardness and toughness. (Figure 4.7-1)

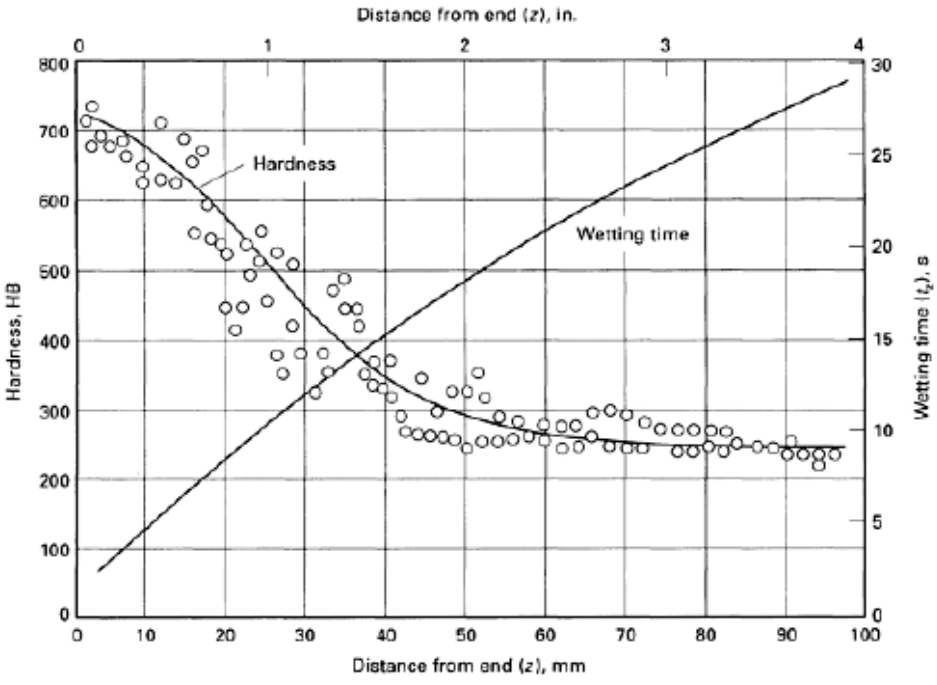

Figure 4.7-1 Wetting time (time water-surface contact without oxide generation) vs distance from the tip. (17)

In conclusion although it is fancy looks G59 had great strength, although with many defects but it still, besides being an accessory, remains proof of great metallurgical skills for the XVI century.

4.8 FEM

4.8.1 FEM Introduction

This chapter will discuss a **FEM thermal model** of the ***quenching*** *process* developed for the sword. The commercial software **COMSOL** has been used for the thermal physical analysis while **Solidworks** have been adopter for the 3D model creation.

4.8.2 The Solidworks Model

Measurements (Figure 4.8-1) have been taken on site in the moment of the delivery of the sword at the Museum in Brescia.

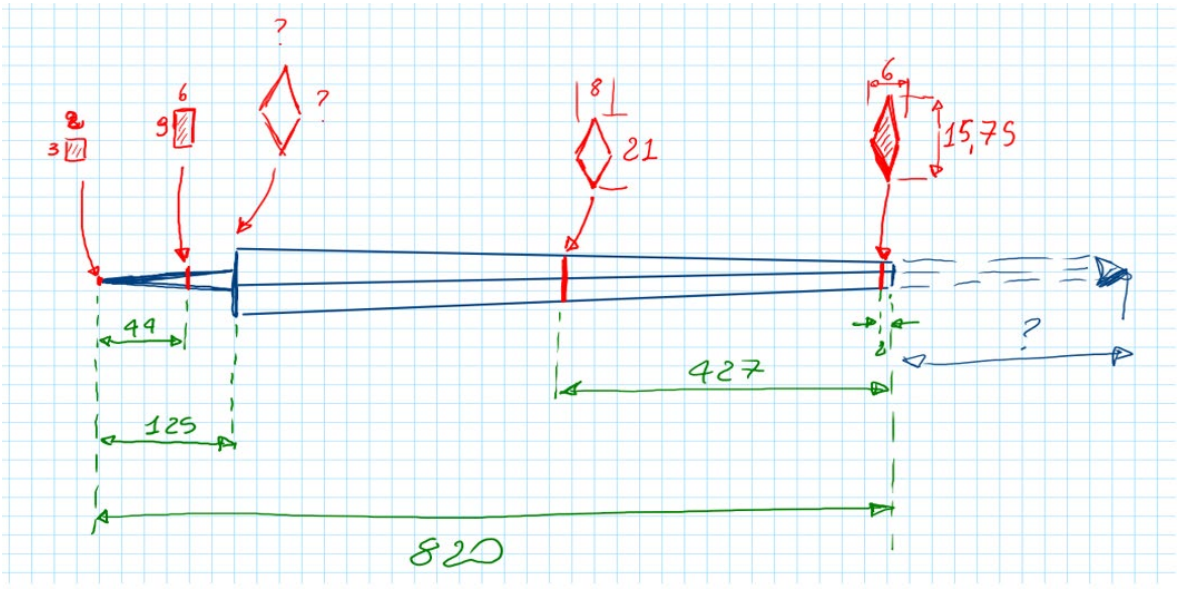

Figure 4.8-1 Sword Measurements on a sketch

Afterwards the sketches have been translated into a solidworks model ready to be injected in COMSOL Multiphysics.

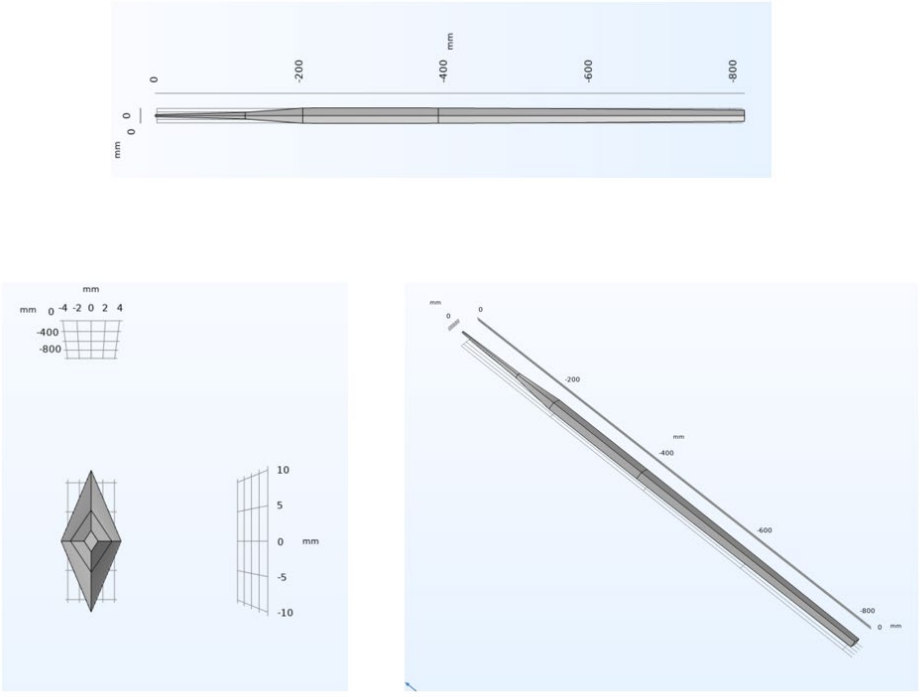

Figure 4.8-2 Final Solidworks Geometry of The Model

4.8.3 Thermal-Phase Model COMSOL

The goal of this FEM model was to describe the **quenching and self-tempering** of the sword. Thus, supposing that the temperature at the start of the quenching was 1200K (to have all austenite), then quenching in cold water(20°C) until Ms is reached in the material and finally leaving the sword self-temper at room temperature until the temperature uniforms.

A Thermal model of quenching have been developed considering the following PDE:

$$\rho c_p \frac{\partial \mathrm{T}}{\partial \mathrm{t}} + \rho c_p \mathbf{u} \cdot \nabla \mathrm{T} + \nabla \cdot \mathbf{q} = Q + Q_{ted} \qquad 4.8\text{-}1$$

Conduction $$\mathbf{q} = -\mathrm{k}\nabla \mathrm{T} \qquad 4.8\text{-}2$$

Convection $$\mathrm{Q} = \mathrm{h}(\mathrm{T}_{ext} - \mathrm{T}) \qquad 4.8\text{-}3$$

Austenite decomposition **in martensite** (diffusionless instant) can be summarized by the Koistinen-Marburger model:

γ→M $$\xi^d = \xi^s{}_0 \cdot (1 - e^{-\beta(M_s - T)}) \qquad 4.8\text{-}4$$

Where ξ^d the phase transformed in martensite, $\xi^s{}_0$ is the equilibrium phase, β is[1/K] the Koistinen-Marburger coefficient and M_s is the Martensite Start temperature[K].

Austenite decomposition **in Bainite, Pearlite** and **Ferrite (**with carbon diffusion**)** can be summarized by the Leblond-Devaux (35) model:

γ→B
γ→α
γ→P

$$\dot{\xi}^d = K(T)\xi^s - L(T)\xi^d \; OR \; \xi^d = \xi^d{}_{eq} \cdot (1 - e^{-\frac{t}{\tau_{s\to d}}}) \qquad 4.8\text{-}5$$

Where the kinetic parameters K(T) and L(T) are function of the temperature described by the following tables calculated by COMSOL itself.

The $\tau_{s\to d}$ is a very important coefficients because it represents the characteristic time of the transformation.

The $-\frac{\mathbf{1}}{\boldsymbol{\tau_{s\to d}}}$ term is representing the speed or decay rate at which the source phase is transforming to the destination phase.

The minus sign in front of it is necessary for convergence.

The higher this number at a given temperature the faster the reaction it is going to be at that temperature. (Figure 4.8-3)

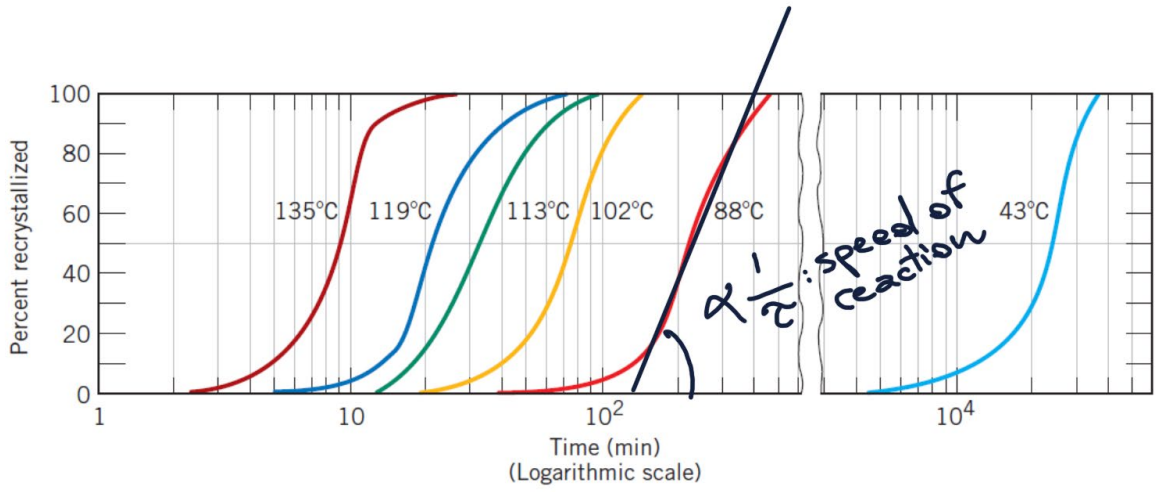

Figure 4.8-3 Phase Transformation evolution representation. (36)

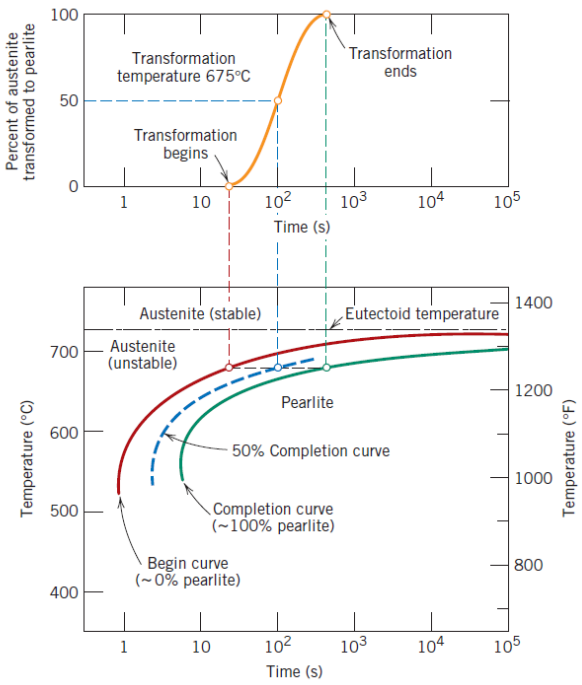

Figure 4.8-4 Example of TTT derivation from a phase transformation exponential evolution.

The K(T), L(T), $\tau_{s\to d}$ coefficients should be either extracted at each temperature level by an experimental TTT or by a calibration procedure trying to minimize a goal function.

TABLE 1: AUSTENITE TO FERRITE, TEMPERATURE-DEPENDENT FUNCTIONS.

Temperature (°C)	K (1/s)	L (1/s)
450	0	0
620	0.005	0.001
750	0	0

TABLE 2: AUSTENITE TO PEARLITE, TEMPERATURE-DEPENDENT FUNCTIONS.

Temperature (°C)	K (1/s)	L (1/s)
450	0	0
550	0.015	0.001
750	0	0

TABLE 3: AUSTENITE TO BAINITE, TEMPERATURE-DEPENDENT FUNCTIONS.

Temperature (°C)	K (1/s)	L (1/s)
450	0	0
620	0.005	0.001
750	0	0

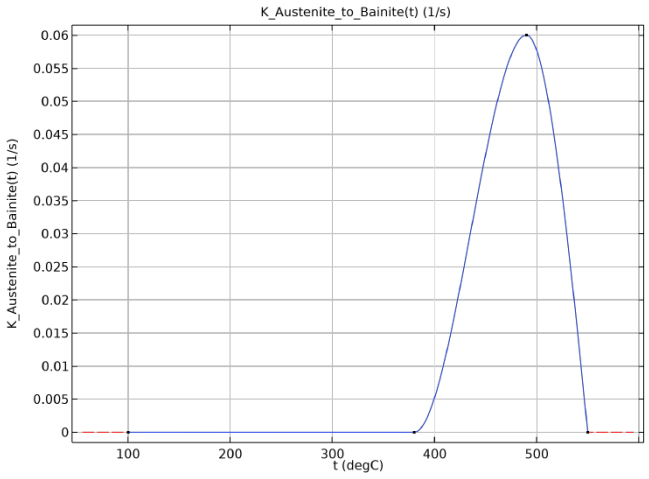

Figure 4.8-5 On the Left tables of K(T) and L(T). On the Right the shape of tables has been plotted.

Noteworthy the Lebond-Devoux comes from the general JMAK formulation with the Avrami index equal to 1.

4.8.4 Results

The following **3 points** were subject to a phase analysis:

1. **Tang**
2. **Interface Water-Air**
3. **End of the blade**

The model predicted the **Tang** to be 40% Bainite, 22% Pearlite, 2% Martensite, 1% Ferrite, 0.8% Austenite at room temperature. (Figure 4.8-6)

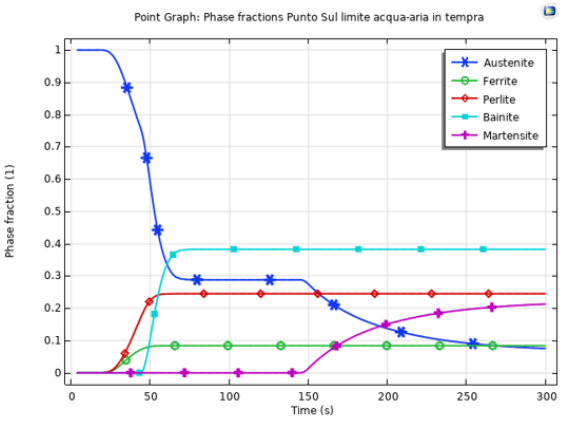

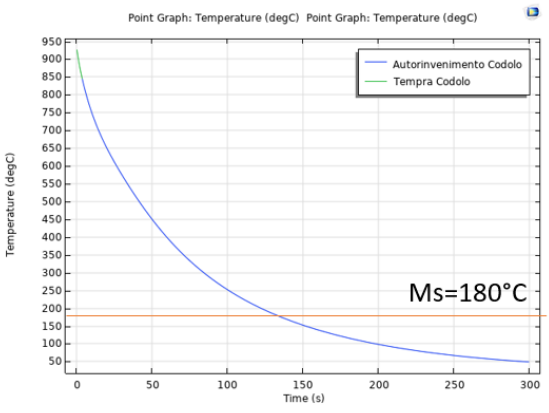

Figure 4.8-6 The red point on top, its composition (left bottom) and its temperature profile (right bottom)

The model predicted the **Interface Water-Air** to be 60% Bainite, 15% Pearlite, 18% Martensite, 0.1% Ferrite, 0.6% Austenite at room temperature. (Figure 4.8-7)

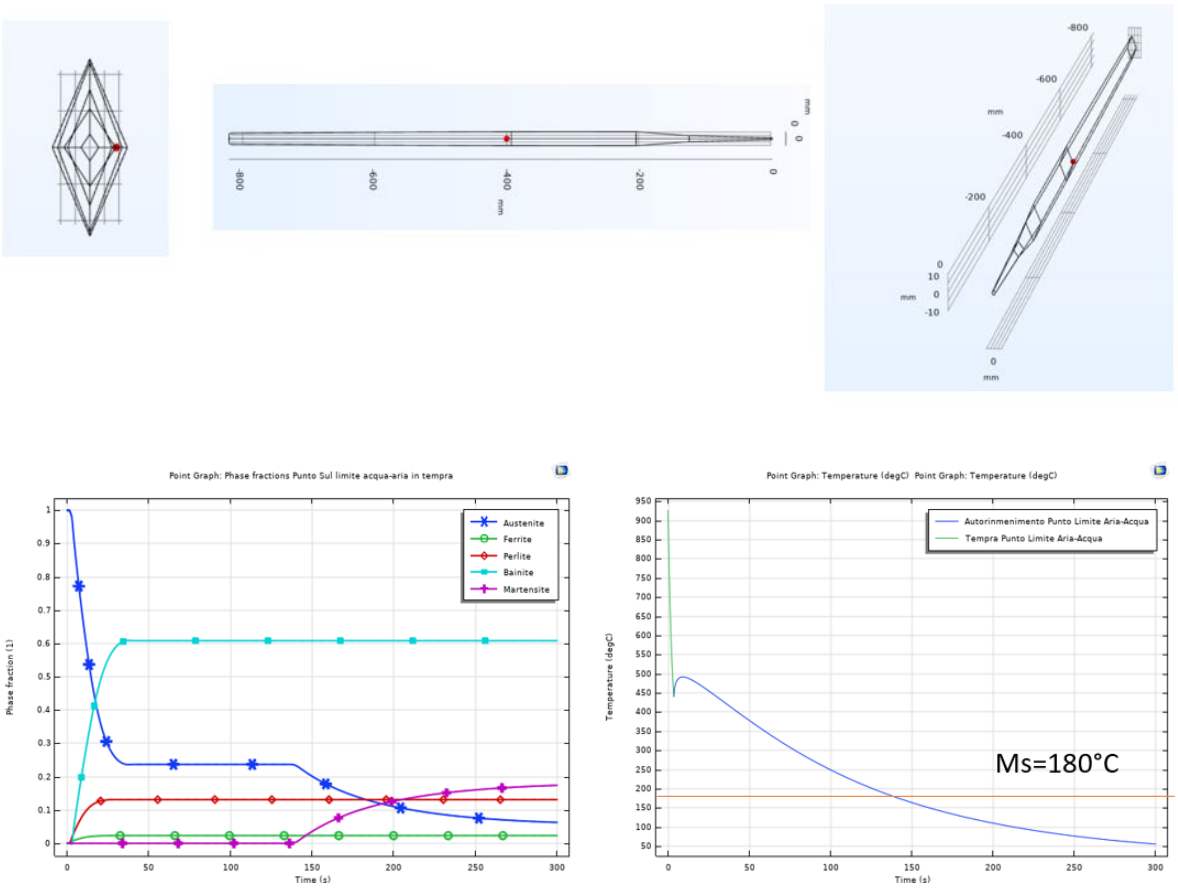

Figure 4.8-7 The red point on top, its composition (left bottom) and its temperature profile (right bottom)

The model predicted the **End of Blade** to be 25 % Bainite, 2.5% Pearlite, 70% Martensite, 2.5% Ferrite, 25% Austenite at room temperature. (Figure 4.8-8)

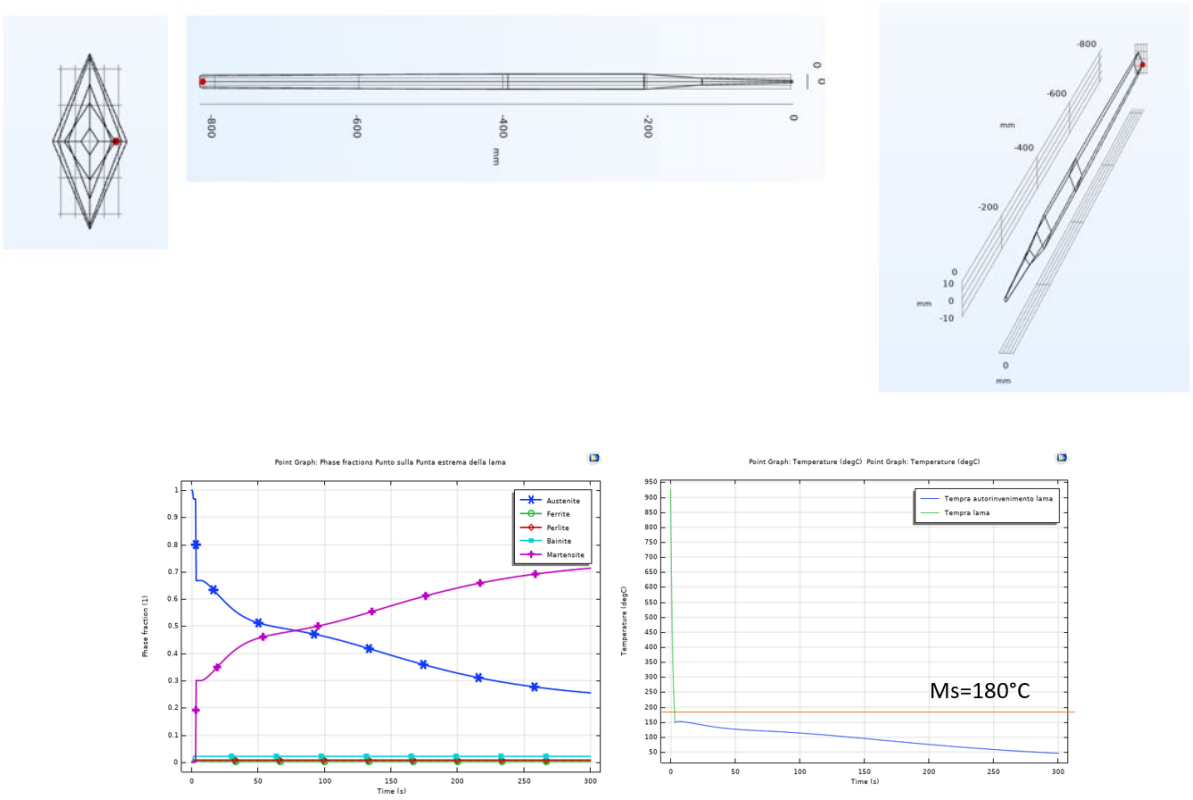

Figure 4.8-8 The red point on top, its composition (left bottom) and its temperature profile (right bottom)

Looking at the temperature profiles all phase transformation diagrams have the martensite content spiking around the martensite start temperature (**Ms**).

Moreover, the parts of the blade that experience the most abrupt temperature change like the tip of the blade have the most Martensite concentration.

This can be explained looking at the CCT diagram developed for this model. (**Figure 4.8-9**)

In fact, since the tip cools it could be described by the most **left curve,** this could be congruent with the fact that there is lots of Martensite when looking at the microscope.

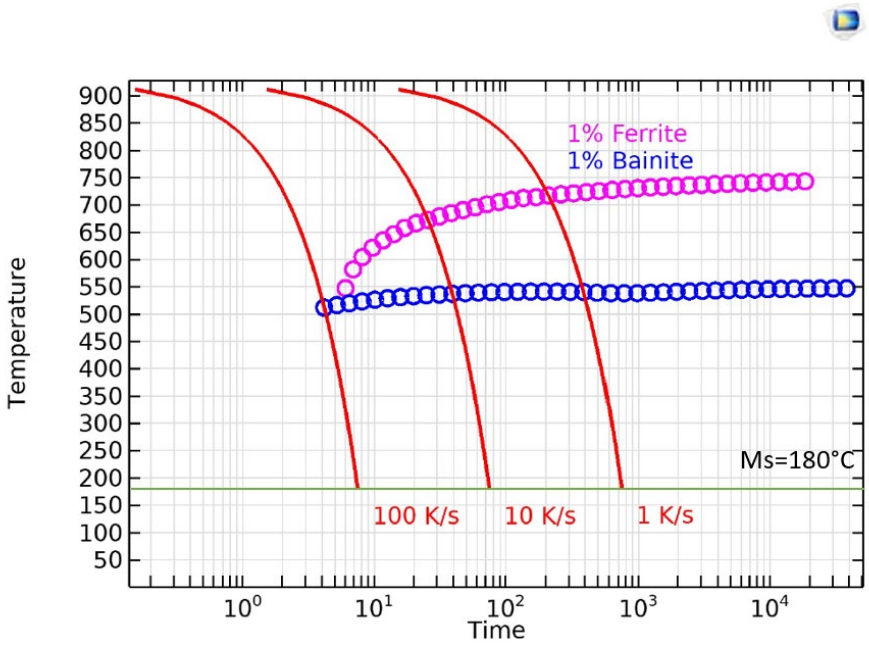

Figure 4.8-9 CCT diagram of the sword's COMSOL general steel material.

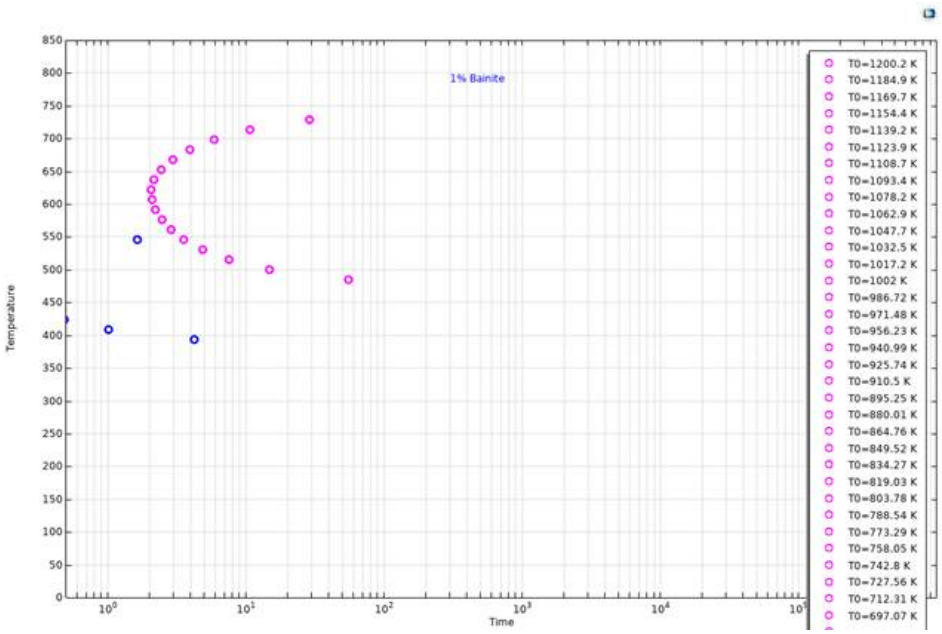

Figure 4.8-10 TTT diagram of the sword's COMSOL general steel material.

The *same kind of considerations* can be done for **all the other parts of the sword**.

Notably looking at the temperature profile time where Ms (martensite start) gets reached after the phase composition remarkably changes.

This is because when the sword gets removed from the quenching water the tang is still warmer than the blade.

Thus, a thermal flux of heat transfer takes place from the tang to the blade.

This phenomenon causes the "**self-tempering**" of the metal together with the changes in phase after Ms start temperature.

Again, the production of this type of swards followed 2 steps that have been modelled:

1. ***Quenching***

2. ***Self-Tempering***

The first is important to form hard Martensite while the second to increase the ductility and decrease brittleness. (Figure 4.8-11)

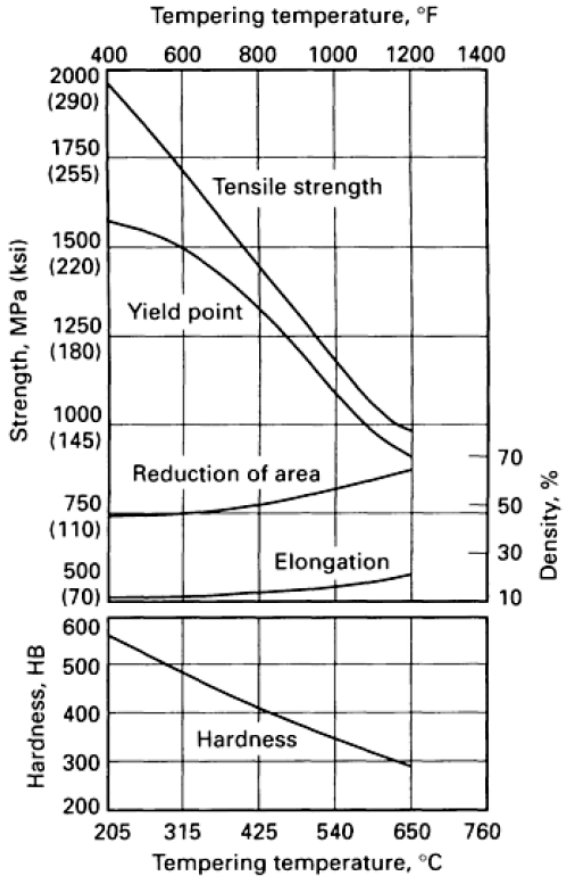

Figure 4.8-11 Effect of tempering temperature on material proprieties. (17)

This is due to the fact the **martensite** when *temperature increases* tend to stabilize its shape *transforming into ferrite* or producing carbides or generating bainite depending on the tempering temperature levels. (Figure 4.8-12)

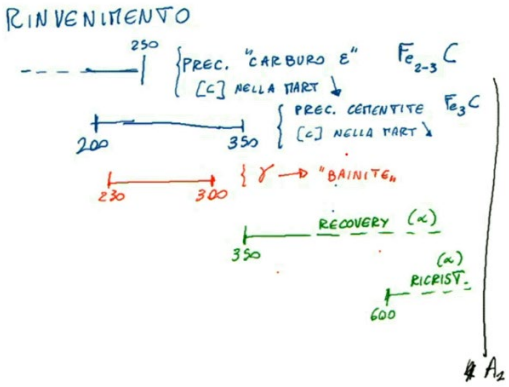

Figure 4.8-12 Martensite behaviour as function of different tempering temperatures. (37)

4.8.5 Discussion

Comparing the FEM model results in terms of phases in the final microstructure the following remarks can be made.

The **Middle of the blade** shows a **ferrite+cementite** microstructure at the microscope since the manufacturers did not reach austenitizing temperature homogeneously along all the parts of the blade.

Thus, the FEM model did not predict the existence of such phases since it assumed of having reached **A1** at the beginning of the process. (Figure 4.8-13)

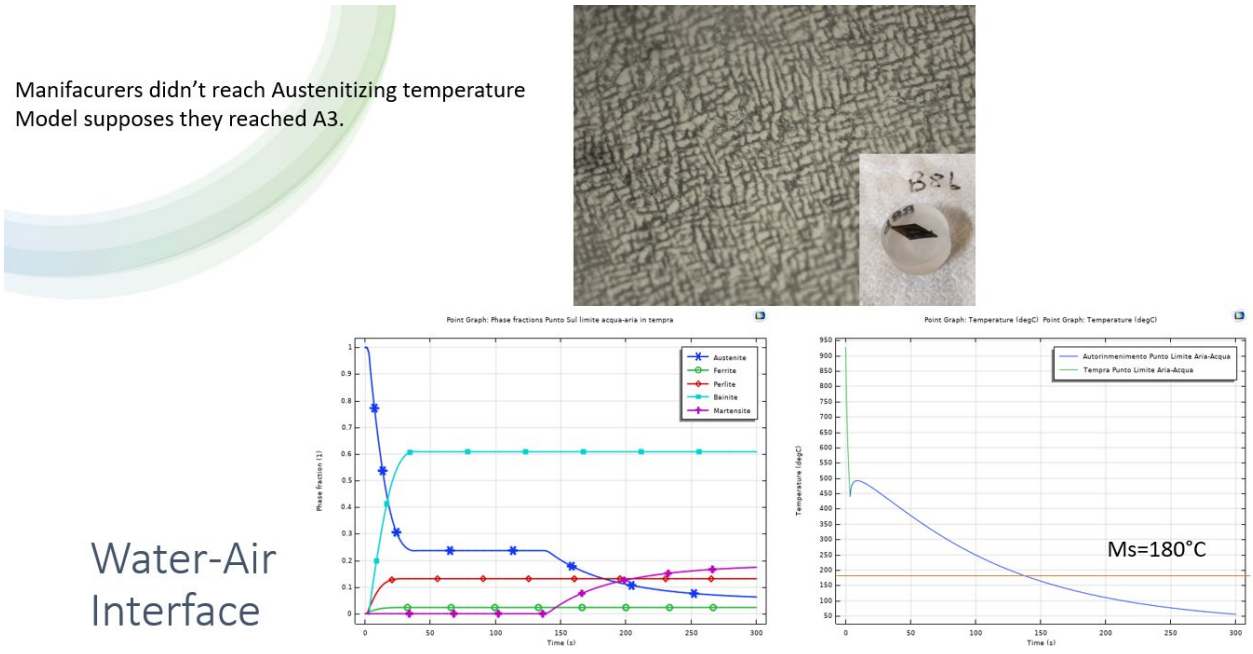

Figure 4.8-13 Microscopy of B8 (Top) and Phase and Temperature profile (Bottom)

Indeed, by changing the initial conditions of the model thus starting at a temperature of 400K and proceeding with quenching and self-tempering the new phase composition graphs have been obtained. (Figure 4.8-14)

Lastly this phase diagram shows high percentage of **ferrite** as one could expect.

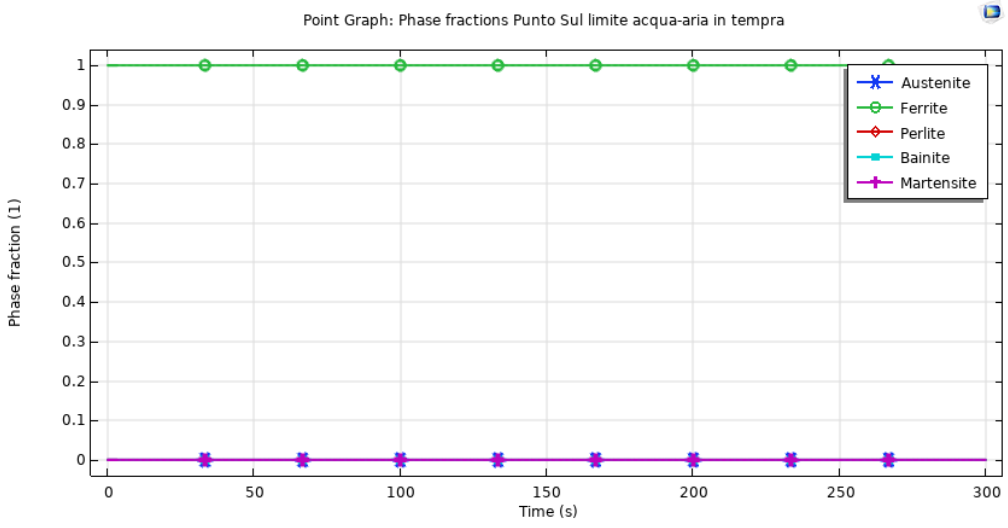

Figure 4.8-14 Phase and Temperature profile

At **the End of the blad**e the FEM model was able to predict the presence of **Martensite** in high percentage. (Figure 4.8-15)

However, it did not predict **Bainite** to be present in the final composition this can be since the real blade tip was lost and our **B1b** sample was from a cut lower than the actual tip of the blade thus containing more **Bainite** since this area experienced a higher self-tempering temperature.

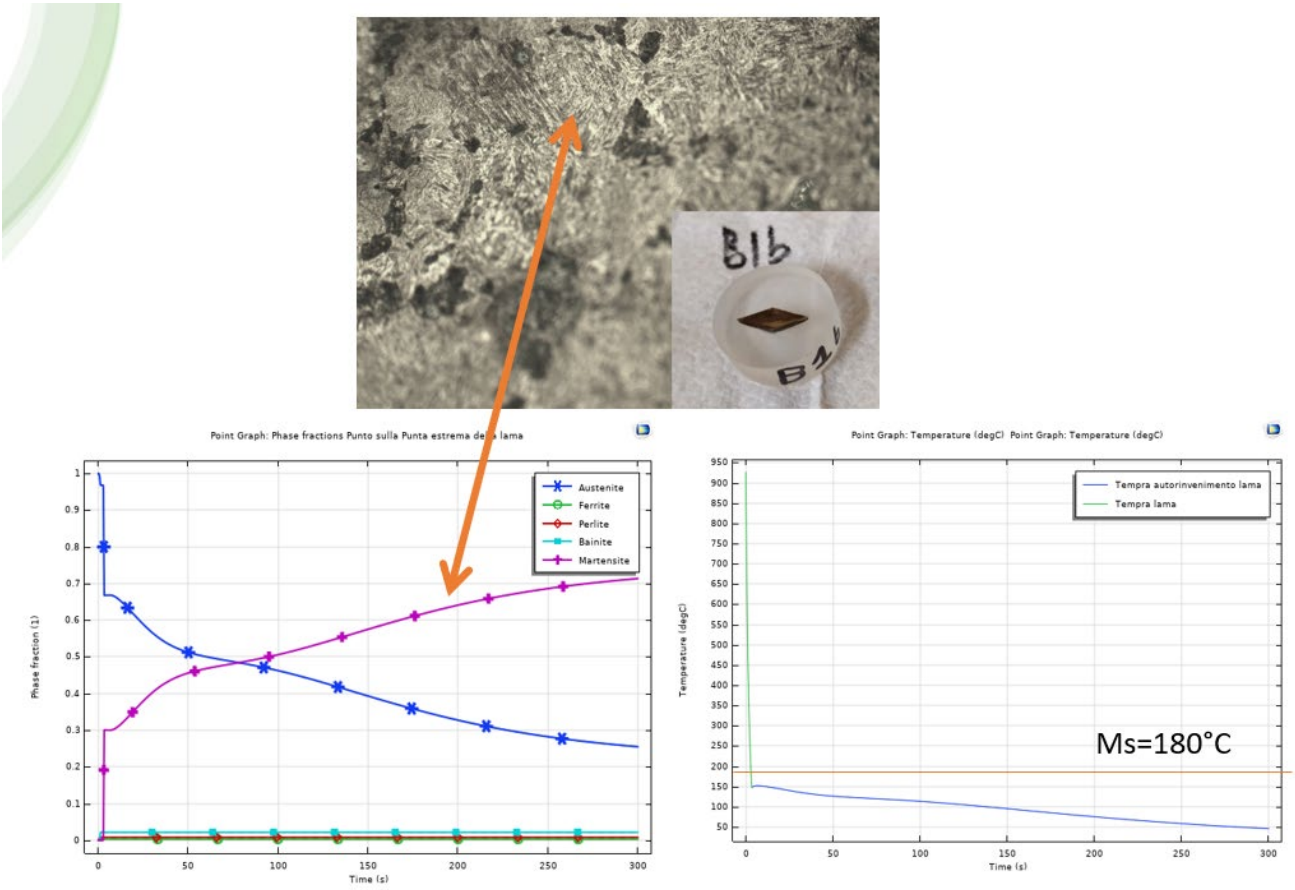

Figure 4.8-15 Microscopy of B1b (Top) and Phase and Temperature profile (Bottom)

4.8.6 Conclusion

This chapter analysed the problem of sword making process identification from a FEM point of view. After defining the boundary conditions, mesh, material of the sword the temperature the fem model was able to solve the temperature profile and the metallographic phase composition of any point at any time during the quenching and self-tempering process quite a quite good degree of approximation.

Comparing the output of the FEM with what saw by eye in the optical microscope some metallographic structures matched.

Of course, the FEM created did not consider all possible parameters from the steelmaking to the final quenched steel and optical metallurgy together with hardness analysis and SEM remain more reliable, but it gives a big picture view of the process.

5 Conclusion

The goal of this work was to study the microstructure and hardness of a civil engineer steel and of an XVI sword from two very different periods in human history such as the end of the Medieval era and the 1st industrial revolution.

In particular this has been carried out by investigated the materials microstructures with an optical microscope. (*Chapter 2*)

The tie-rod had areas at different carbon content showing mainly zones of pearlite, cementite and ferrite combinations which lead to believe it had a slow cooling.

Moreover, the carbon inhomogeneities may be due to a temperature gradient the final forging.

Furthermore, in *Chapter 2* a second phase extraction followed by an analysis at optical and SEM microscopes have been object of study.

In addition to EDS analysis on the inclusion's composition showed a really low sulphur content together with the presence of particular oxides that suggest that the tie-rod was produced from the bloomery process (direct method).

This is important because not only the inclusions give away the 'quality' of a metal but also the skill of the manufacturer.

Furthermore, in *Chapter 2* a FEM Thermal-Phase model of the quenching and self-tempering of the sword have been to model the hypnotized production method from *Chapter 3*.

The model showed a prevalent martensitic microstructure towards the end of the blade that is congruent with the actual metallographic inspection at the optical microscope.

5 Conclusion

The goal of this work was to study the microstructure and hardness of a civil engineer steel and of an XVI sword from two very different periods in human history such as the end of the Medieval era and the 1st industrial revolution.

In particular this has been carried out by investigated the materials microstructures with an optical microscope. (*Chapter 2*)

The tie-rod had areas at different carbon content showing mainly zones of pearlite, cementite and ferrite combinations which lead to believe it had a slow cooling.

Moreover, the carbon inhomogeneities may be due to a temperature gradient the final forging.

Furthermore, in *Chapter 2* a second phase extraction followed by an analysis at optical and SEM microscopes have been object of study.

In addition to EDS analysis on the inclusion's composition showed a really low sulphur content together with the presence of particular oxides that suggest that the tie-rod was produced from the bloomery process (direct method).

This is important because not only the inclusions give away the 'quality' of a metal but also the skill of the manufacturer.

Furthermore, in *Chapter 2* a FEM Thermal-Phase model of the quenching and self-tempering of the sword have been to model the hypnotized production method from *Chapter 3*.

The model showed a prevalent martensitic microstructure towards the end of the blade that is congruent with the actual metallographic inspection at the optical microscope.

Bibliography

1. Wikipedia Iron Ore. [Online] https://en.wikipedia.org/wiki/Iron_ore *visited on* 06/01/2021

2. Charlton, M. F., Blakelock, E., Martinón-Torres, M., & Young, T.(2012). Investigating the production provenance of iron artifacts with multivariate methods. Journal of archaeological Science, 39(7), 2280-2293.

3. Blakelock, E., Martinon-Torres, M., Veldhuijzen, H. A., & Young, T. (2009). Slag inclusions in iron objects and the quest for provenance: an experiment and a case study. Journal of Archaeological Science, 36(8), 1745-1757.

4. Leroy, S. (2010). Circulation au Moyen Âge des matériaux ferreux issus des Pyrénées ariégeoises et de la Lombardie. Apport du couplage des analyses en éléments traces et multivariées (Doctoral dissertation, Université de Technologie de Belfort-Montbeliard).

5. Leroy, S., Simon, R., Bertrand, L., Williams, A., Foy, E., & Dillmann, P. (2011). First examination of slag inclusions in medieval armours by confocal SR-μ-XRF and LA-ICP-MS. Journal of Analytical Atomic Spectrometry, 26(5), 1078-1087.

6. Brack, H.G.(2008).Steel and Toolmaking Strategies and Techniques Before 1870.Pennywheel Press

7. Iron smelting in Middle-Age, from "De Re Metallica" by Georgius Agricola, 1556. 1556.

8. Wikipedia Iron Smelting. [Online] https://commons.wikimedia.org/wiki/File:CNX_Chem_19_01_BlastFurn.png *visited on* 03/02/2021.

9. Sims, L. (2006). The Backyard Blacksmith: Traditional Techniques for the Modern Smith (p. 184). Quarry Books.

10. Wikipedia. Indirect_reduction_of_steel. [Online] https://marspedia.org/ Indirect_reduction_of_steel. *visited* on 03/01/2021.

11. —. Bessemer_process. [Online] https://en.wikipedia.org/wiki/Bessemer_process *visited* on 01/02/2021.

12. Slag. [Online] https://en.wikipedia.org/wiki/Slag. *visited* on 02/01/2021.

13. Matteis, P., Scavino, G., & Ferro, G. (2019). Characterization and Joining of an Historical Ferrous Tie-Rod. International Journal of Architectural Heritage, 13(3), 472-484.

14. How were Swords Made. [Online] http://www.thearma.org/essays/

How_Were_Swords_Made.html *visited on* 06/02/2021

15. Boniardi, M., & Casaroli, A. (2017). Metallurgia degli acciai. Gruppo Lucefin. Esine (Brescia), Italia, 1.

16. Bain, E. C., & Paxton, H. W. (1966). Alloying elements in steel. 1966, 291 P. AMERICAN SOCIETY FOR METALS, METALS PARK, OHIO.

17. Hardesty, F. (1983). Metals handbook, volume 4: Heat treating: prepared under the direction of the Handbook Committee and planned, prepared, organised, and reviewed by the Heat Treating Division, ASM, Metals Park, Ohio, 1981. ISBN 1-87170-010-7, xix+ 826 pages, illustrated, hard cover£ 44.50.

18. Aliya, D., Adams, B. L., & Alman, D. (2018). ASM Handbook Volume 9 Metallography and Microstructures.

19. NPTEL. [Online] https://www.youtube.com/watch?v=IPjM4UGumT4 *visited on* 15/01/2021.

20. Nital Wikipedia. [Online] Wikipedia. https://en.wikipedia.org/wiki/Nital *visited on* 16/02/2021 .

21. Graziano, Ubertalli. Slides corso Materiali, Politecnico, 2019.

22. Wikipedia. Cementite. [Online] https://it.wikipedia.org/wiki/Cementite *visited on* 20/02/2021 .

23. ASTM E194-20, Standard Test Method for Acid-Insoluble Content of Copper and Iron Powders, ASTM International, West Conshohocken, PA, 2020, www.astm.org

24. Kalab, Miloslav. (2015). Microstructure of Bacterial Filters Used as Support in Scanning Electron Microscopy. 10.13140/RG.2.1.3340.5606.

25. Microscopes | Bio Ninja. [Online] https://ib.bioninja.com.au/standard-level/topic-1-cell-

biology/11-introduction-to-cells/microscopes.html *visited on* 12/02/2021 .

26. 2000, Material Science. [Online] https://www.youtube.com/watch?v=GY9lfO-tVfE *visited on* 11/02/2021 .

27. EDX. [Online] http://www.cei.washington.edu/education/science-of-solar/energy-dispersive-x-ray-spectroscopy/ *visited on* 06/02/2021 .

28. Shomu. Electron Microscopy | SEM. [Online] https://www.youtube.com/watch?

v=VdNhREmkrmE *visited on* 12/01/2021 .

29. Vello, M., & Tonin, F. (2018). I grandi spadai feltrini e bellunesi. Youcanprint.

30. Merlo, M., Tosin, L., & De Vita, C. (2011). Le armi antiche: Bibliografia ragionata nel Servizio Bibliotecario Nazionale. Gangemi Editore spa.

31. Merlo, M., Tosin, L., & De Vita, C. (2011). Le armi antiche: Bibliografia ragionata nel Servizio Bibliotecario Nazionale. Gangemi Editore spa., p. 58 Tav.18. 85

32. York, Metropolitan Museum of Arts of New. [Online]

https://www.metmuseum.org/art/collection/search/35679?searchField=All&sortBy=Relevance&when=A.D.+1400-1600&what=Swords&ft=Italian&offset=0&rpp=20&pos=1 visited on 16/02/2021.

33. myarmoury. Feature arms rapier. [Online]

http://myarmoury.com/feature_arms_rapier.html *visited on* 01/02/2021 .

34. Allen, C. M., & Boardman, B. (2005). ASM handbook, volume 1, properties and selection: irons, steels, and high performance alloys section: publication information and contributors publication information and contributors. Fonderie, 1, 1618.

35. Weisz-Patrault, D. (2017). Multiphase model for transformation induced plasticity. Extended Leblond's model. Journal of the Mechanics and Physics of Solids, 106, 152-175.

36. Callister, W. D., & Rethwisch, D. G. (2018). Materials science and engineering: an introduction (Vol. 9). New York: Wiley.

37. Note di Materiali Per L'industria Meccanica(Corso Polito). Matteis, Paolo.

38. TV, Hitachi High-Tech Global. [Online] https://youtu.be/cAKcOyrt5Vc.

39. Li, M. V., Niebuhr, D. V., Meekisho, L. L., & Atteridge, D. G. (1998). A computational model for the prediction of steel hardenability. Metallurgical and Materials transactions B, 29(3), 661-672.

40. American Society for Metals. (1977). Atlas of isothermal transformation and cooling transformation diagrams. American Society for Metals.

41. Wikipedia Rapier. [Online] https://en.wikipedia.org/wiki/Rapier *visited on* 06/02/2021 .

42. Eppelbaum, L. V., & Pilchin, A. N. (2006). Iron and its unique role in Earth evolution.

43. Lotzof, Kerry. The heavy metal rock bands charting life on early Earth. [Online] https://www.nhm.ac.uk/discover/the-heavy-metal-rock-bands-charting-life-on-early-earth.html#:~:text=Around%202.6%20billion%20years%20ago,layers%20of%20silica%2Drich%20silt *visited on* 03/02/2021 .